Myosin light chain 3 serves as a receptor for nervous necrosis virus entry into host cells via the macropinocytosis pathway

Authors: Lan Yao[1,2,3†], Wanwan Zhang[1,2,3,†], Xiaogang Yang[1,2,3], Meisheng Yi[1,2,3*], Kuntong Jia[1,2,3*]

Affiliations:

[1]School of Marine Sciences, Sun Yat-sen University, Guangzhou 510000, China.

[2]Southern Marine Science and Engineering Guangdong Laboratory (Zhuhai), Zhuhai 519000, China.

[3]Guangdong Provincial Key Laboratory of Marine Resources and Coastal Engineering, Guangzhou 510000, China.

†These authors contributed equally to this work.

*Corresponding author. Email: jiakt3@mail.sysu.edu.cn; yimsh@mail.sysu.edu.cn

Abstract: *Nodaviridae* infections cause severe mortality in insects and fish, with nervous necrosis virus (NNV) posing significant threats to global fish populations. However, the host factors involved in NNV entry remain poorly understood. Here, we identify myosin light chain 3 from marine medaka (*Oryzias melastigma*) (MmMYL3) as a novel receptor for red-spotted grouper NNV (RGNNV), facilitating internalization via macropinocytosis. MmMYL3 directly binds the RGNNV capsid protein (CP), which dependents on the arm and S domains of CP and the EF-hand2 domain of MmMYL3. In vitro experiments showed that MmMYL3 siRNA, protein, anti-MYL3 antibodies or the arm domain synthetic peptides blocked RGNNV entry. Moreover, in vivo administration of MmMYL3 protein also inhibited RGNNV infection. Ectopic MmMYL3 expression enabled RGNNV internalization into resistant cells. Notably, MmMYL3 facilitated RGNNV internalization through the macropinocytosis pathway via the IGF1R-Rac1/Cdc42 axis. Collectively, our findings underscore MYL3's crucial role in NNV entry and its potential as an antiviral target.

Keywords: *Nodaviridae*; nervous necrosis virus; myosin light chain 3; macropinocytosis; receptor

Introduction

Viral encephalopathy and retinopathy, also known as viral nervous necrosis, is a highly contagious and pathogenic disease that infects more than 120 marine and freshwater fish species, leading to mass mortalities and severe economic losses in the aquaculture industry. The etiological agent responsible, nervous necrosis virus (NNV), belongs to the *Nodaviridae* family, genus *Betanodavirus* and manifests as a nonenveloped single-stranded RNA virus (Costa and Thompson, 2016; Munday et al., 2002). The NNV genome is composed of two RNA segments: RNA1 encodes the RNA-dependent RNA polymerase (RDRP), while RNA2 encodes the viral capsid protein (CP), which plays a critical role in the initial interaction with host cell surface receptors, thus facilitating viral entry (Bandín and Souto, 2020; Mori et al., 1992).

Viral entry into host cells is a key determinant of host specificity, tissue tropism, and viral pathogenicity, and involves intricate interactions between viral capsid proteins and host cell receptors (Grove and Marsh, 2011). Viruses utilize sophisticated strategies to attach to one or multiple receptors, enabling them to cross the plasma membrane and access the necessary host cell machinery (Melissa S. Maginnis, 2018). Viral receptors function not only as attachment moieties but also as entry factors, coordinators of viral trafficking, and activators of signaling events (Marsh and Helenius, 2006). Therefore, identifying virus receptors and understanding the mechanism of virus-receptor interaction is critical for better preventing viral diseases. Although NNV exhibits a broad host tropism, only heat shock cognate protein 70 (HSC70) , heat shock protein 90ab1 (HSP90ab1) and Nectin1 have been identified as its receptor or co-receptor (Chang and Chi, 2015; Zhang et al., 2020, n.d.). Following NNV CP protein recognizes the cellular surface receptor, the NNV enters the cell by receptor-mediated endocytosis. Viruses usually take advantage of various endocytic pathways to enter host cells, with clathrin-mediated endocytosis (CME), macropinocytosis, and caveolar/raft-dependent endocytosis being the most extensively studied (Mercer et al., 2010). Previous studies revealed that NNV particles utilize the receptor-mediated CME and macropinocytosis internalization pathways to invade host cells (Liu et al., 2005), with the former facilitated by HSP90ab1

and HSC70 (Zhang et al., 2020). However, the receptor responsible for mediating NNV invasion of host cells through macropinocytosis remains unknown.

Among the diverse cellular factors that can serve as viral receptors, members of the myosin family have emerged as intriguing candidates (He et al., 2022). The myosin family comprises a wide range of actin-associated motor proteins that play a role in a variety of cellular activities, including signal transduction, intracellular transport and cell division, etc. Up to date, more than 40 known classes of myosin have been identified (Foth et al., 2006). Recent studies underscore their significance in various viral infections. For instance, myosin heavy chain 9 has been identified as a crucial factor for various virus infection (Li et al., 2018). Non-muscle myosin heavy chain IIA serves as a functional entry receptor for herpes simplex virus-1 (Arii et al., 2010). Additionally, myosin II light chain activation is essential for influenza A virus cell entry through macropinocytosis (Banerjee et al., 2014).

Myosin light chain 3 (MYL3), a constituent of the myosin light chain family predominantly found in muscle tissues, particularly the heart and skeletal muscles, plays a pivotal role in muscle contraction by forming the myosin complex with myosin heavy chain and facilitating actin filament sliding (Ingles et al., 2005; Zhang et al., 2016). Mutations in the MYL3 gene have been associated with various muscle-related disorders, including cardiomyopathies and skeletal muscle myopathies (Mavilakandy and Ahamed, 2022). However, the role of MYL3 in virus infection remains undiscovered. Huang et al reported that *Epinephelus coioides* MYL3 might interact with native NNV CP by proteomic analysis of immunoprecipitation (IP) assay (Huang et al., 2020), yet its involvement in NNV infection, particularly its role in viral invasion, remains uncertain.

In this study, we unveil MYL3 of marine medaka (*Oryzias melastigma*) (MmMYL3) as a novel NNV entry receptor, elucidating its facilitation of RGNNV entry into host cells through macropinocytosis, mediated by the IGF1R-Rac1/Cdc42 pathway. These findings offer novel insights into the intricate mechanisms underlying NNV entry and highlight potential targets for the development of antiviral drugs.

Results

Interaction between MmMYL3 and CP

First, a Co-IP assay was conducted to validate the interaction between MmMYL3 and CP. MmMYL3 exhibited colocalization and co-precipitation with CP (Fig. 1, A and B). GST-tag pull-down assays provided additional confirmation of the direct interaction between MmMYL3 and CP, as well as MmMYL3 and RGNNV virions (Fig. 1, C and D). SPR analysis further confirmed a direct interaction between MmMYL3 and CP, with kinetics revealing association rate constant (Ka), dissociation rate constant (Kd), and equilibrium dissociation constant (K_D) of 1.448×10^4 M^{-1} s^{-1}, 1.679×10^{-4} s^{-1}, and 2.95 μM, respectively (Fig. 1E). Additionally, the interaction between CP and MYL3 was consistently observed in another marine fish species, *Lateolabrax japonicus* (Fig. 1F). These results robustly affirm the binding affinity of MmMYL3 to CP.

Domain mapping of the association between MmMYL3 and CP

To delineate the domain of MmMYL3 required for interaction with CP, various Myc-tagged distinct domains of MmMYL3 were constructed, and Co-IP assays revealed that deletion of the EF-hand2 domain of MmMYL3 abolished its interaction with CP, suggesting the essential role of the EF-hand2 domain (Fig. 1, G and I). Furthermore, to ascertain which domain of CP is necessary for interaction with MmMYL3, we generated a series of Myc-tagged CP deletion mutants (Fig. 1H). Co-IP assays revealed that deletion of the arm domain and S domain of CP resulted the abrogation of its interaction with MmMYL3 (Fig. 1J). Collectively, these findings indicate that MmMYL3 interacts with the arm and S domain of CP through its EF-hand2 domain.

Localization of MmMYL3 on the cell surface

We next explored whether MmMYL3 is present on the cell surface, a prerequisite for a functional viral receptor. Immunofluorescence (IF) assays in permeabilized and non-permeabilized hMMES1 and HEK293T cells transfected with Myc-MmMYL3 revealed MmMYL3 localization both at the cell surface and in the cytoplasm (Fig. 2, A and B). Meanwhile, no immunofluorescent signal was detected on the surface of non-permeabilized cells using anti-Actin abs. Conversely, in permeabilized cells treated with

Triton X-100, MmMYL3 proteins were found not only on the cell surface but in the cytoplasm. To corroborate the cell surface localization of MmMYL3, a protease protection assay was carried out. Besides, the addition of proteinase K resulted in the significant reduction of MmMYL3 protein in nonpermeabilized HEK293T or hMMES1 cells transfected with pCMV-Myc-MmMYL3 plasmid compared to the control without proteinase K treatment (Fig. 2, C and D), confirmed that MmMYL3 is exposed on the surface of these cells.

To visualize the colocalization of MmMYL3 with the cell membrane, PKH 26, a red fluorescent dye that binds stably to the lipid region of the cell membrane, was used. Colocalization of MmMYL3 with PKH 26 in hMMES1 cells was observed, further corroborating its membrane association (Fig. 2 E). Flow cytometry analysis using Alexa Fluor 488-conjugated anti-Myc antibody also indicated a proportional increase in MmMYL3 surface expression with increasing MmMYL3 concentrations in HEK293T and hMMES1 cells (Fig. 2F). Lastly, co-transfection of MmMYL3 with the membrane protein Na^+/K^+-ATPase alpha 1 (ATP1A1) in HEK293T and hMMES1 cells showed clear colocalization of MmMYL3 with ATP1A1 in both permeabilized and non-permeabilized conditions (Fig. 2, G and H), further affirming the presence of MmMYL3 on the cell surface. Collectively, these findings robustly demonstrate that MmMYL3 is localized on the cell surface.

MmMYL3 serves as a surface receptor of RGNNV

To investigate whether MmMYL3 was involved in RGNNV infection, we first examined the expression pattern of *MmMYL3* during RGNNV infection. *MmMYL3* exhibited a significant highly expression from 2 to 48 hours post infection (hpi), peaking at 4 hpi, indicating MmMYL3 might play a vital role in the early stages of RGNNV infection (fig. S1). Ectopic expression of MmMYL3 significantly increased *CP* expression and RGNNV titer (Fig. 3, A to C), while MmMYL3 knockdown resulted in decreased *CP* gene transcription and virus titer (Fig. 3, D to F).

To further substantiate that MmMYL3 functions as a receptor for RGNNV infection, commercial anti-human MYL3 abs and purified GST-tagged MmMYL3 proteins were used to evaluate the role of MmMYL3 in the virus entry process. Notably, recombinant MmMYL3 (fig. S2) proteins significantly reduced the entry of RGNNV into hMMES1 cells in a dose-dependent manner (Fig. 3, G and H) and treatment with anti-MYL3 abs (fig. S3) resulted in a significant reduction in *CP* and *RDRP* levels at 2 and 4 hpi, suggesting inhibition of RGNNV entry (Fig. 3, I and J). Moreover, synthetic peptides derived from the arm domain of CP could block RGNNV entry in a dose-dependent manner (Fig. 3, K and L).

Cellular receptors required for virus infection confer infectability when they are expressed in an uninfectable cell type. To further demonstrate the receptor function of MmMYL3, we tested whether overexpression of MmMYL3 could render typically resistant cells susceptible to RGNNV infection. HEK293T cells, which are not naturally permissive to RGNNV, were transfected with MmMYL3 or MmHSP90ab1 (a known NNV receptor). First, we detected CP anti-reverse sequences (*CP (-)*), which is a replicative intermediate for production of viral RNAs, in MmMYL3 or MmHSP90ab1-overexpressing HEK293T cells post RGNNV infection, but not in empty vector transfected cells (Fig. 4A). Similar with MmHSP90ab1, overexpression of MmMYL3 promoted the entry of RGNNV into HEK293T cells (Fig. 4B). Additionally, like observations in hMMES1 cells, abundant viral particles were observed in the cytoplasm of MmMYL3 overexpressing HEK293T cells post RGNNV infection (Fig. 4C). The internalization of RGNNV into MmMYL3 overexpressing HEK293T cells was further evidenced by the intracellular immunofluorescence localization of CP at 24 hpi (Fig. 4D). These results further support the susceptibility conferred by MmMYL3 expression, highlighting its role as a receptor for RGNNV.

MmMYL3 is vital for RGNNV pathogenesis in marine medaka

To evaluate the physiological relevance of MmMYL3 in RGNNV infection, marine medaka were injected with mixtures of RGNNV and recombinant MmMYL3 protein or GST control protein, respectively (Fig. 5A). Fish injected with the MmMYL3-RGNNV

mixture exhibited significantly higher survival rates compared to those injected with the GST-RGNNV mixture (Fig. 5B), indicating a protective effect of MmMYL3 on viral pathogenesis. Consistent with these findings, qRT-PCR analysis showed that CP expression levels in the brain and eye tissues were markedly reduced in the medaka treated with the MmMYL3 protein (Fig. 5C). Furthermore, histopathological analysis revealed reduced pathological injury, in the eyes and brains of the fish treated with MmMYL3 protein, as evidenced by diminished vacuolization compared to the control group (Fig. 5, D and E). These results strongly indicate that MmMYL3 plays a critical role in mediating RGNNV infection and pathogenesis in marine medaka.

Involvement of MmMYL3 in RGNNV Entry via Macropinocytosis

Previous studies have reported macropinocytosis and CME as the primary routes of NNV internalization. To determine whether macropinocytosis is involved in RGNNV entry into hMMES1 cells, we used a panel of compounds to treat the cells prior to viral infection, including EIPA (macropinocytosis inhibitor), Rottlerin (macropinocytosis inhibitor), CPZ (CME inhibitor), and Nystatin (caveolin inhibitor). After treatment, hMMES1 cells were infected with RGNNV, and viral copies in cell lysates were quantified by qRT–PCR. The results indicated that EIPA, Rottlerin, and CPZ significantly inhibited RGNNV infection compared with the dimethyl sulfoxide (DMSO) control (Fig. 6A), whereas Nystatin had no obvious effect, indicating RGNNV enters hMMES1 cells via macropinocytosis and CME pathways.

To clarify the role of MmMYL3 in the process of RGNNV endocytosis, MmMYL3-overexpressing hMMES1 cells were treated with the previously mentioned inhibitors before virus infection. qRT-PCR experiments demonstrated a significant, dose-dependent reduction in internalized RGNNV with EIPA and Rottlerin treatments (Fig. 6B). Fluid-phase uptake is a distinctive feature activated during macropinocytosis. Studies on various viruses entering host cells via macropinocytosis have demonstrated a transient enhancement in fluid-phase uptake (Delpeut et al., 2017). Dextran served as a macropinocytosis marker, being taken up by cells during macropinocytosis. As expected, cells infected with RGNNV displayed dextran-positive vesicles resembling larger,

irregular macropinosomes at 4 hpi, in contrast to mock-infected cells (Fig. 6C). Meanwhile, clusters of MmMYL3 were observed co-localized with RGNNV CP protein in dextran-positive macropinosomes (Fig. 6D). These findings suggest that MmMYL3 facilitated RGNNV enter hMMES1 cells via macropinocytosis.

Involvement of MmIGF1R in MmMYL3-Mediated RGNNV Entry

Macropinocytosis initiation necessitates the coordinated activation of multiple signaling pathways, typically induced by growth factors that prompt the activation of receptor tyrosine kinases (RTKs) (Y. Y. Zhang et al., 2022). To determine whether RTK activation is essential for RGNNV entry mediated by MmMYL3, a series of inhibitors of RTKs were utilized. Inhibitors of IGF1R (AZD-3463, Picropodophyllin) could block MmMYL3-mediated RGNNV entry, but inhibitors of InsR (NVP-TAE), EGFR (Gefitinib) and c-Met (SU11274) had no significant effect on virus entry mediated by MmMYL3 (Fig. 7A). To further clarify the relationship between MmMYL3 and MmIGF1R, MmMYL3-Myc and MmIGF1R-GFP were co-transfected into HEK293T cells, and we found that MmMYL3 were colocalized with MmIGF1R (Fig. 7B). Additionally, Co-IP assay showed that MmIGF1R could interact with MmMYL3 through the extracellular domain (Fig. 7, C and D). Furthermore, pull-down assay further validated the direct interaction between MmMYL3 and MmIGF1R (Fig. 7E). Additionally, overexpression of MmIGF1R promoted the entry of RGNNV, whereas knockdown of MmIGF1R by siRNA inhibited RGNNV entry (Fig. 7, F to I). These results strongly indicate that MmIGF1R is tightly associated with MmMYL3-mediated viral invasion.

Rac1/Cdc42 contributes to RGNNV entry

The Ras superfamily GTPases, particularly Rac1 and Cdc42, are essential regulators of macropinocytosis, contributing to actin cytoskeletal reorganization and membrane ruffling (Bar-Sagi and Feramisco, 1986; Bar-Sagi et al., 1987). We therefore examined the relationship between Rac1, Cdc42 and IGF1R. Co-IP assays revealed the co-precipitation of MmRac1 and MmCdc42 with MmIGF1R (Fig. 8, A and B). Furthermore,

we found that MmRac1 and MmCdc42 could interact with the intracellular region of MmIGF1R (Fig. 8, C and D). In addition, MmRac1 and MmCdc42 were observed to co-localize with MmIGF1R (Fig. 8, E and F). To evaluate the functional significance of MmRac1 and MmCdc42 in RGNNV internalization, hMMES1 cells were transfected with either MmRac1 or MmCdc42. Overexpression of either MmRac1 or MmCdc42 enhanced RGNNV internalization, as demonstrated by increased viral RNA levels (Fig. 8, G to J). In contrast, the specific inhibitors of Rac1 (EHT1864) and Cdc42 (MLS-573151) significantly reduced RGNNV entry in a dose-dependent manner (Fig. 8, K and L).

Actin filaments play a crucial role in facilitating membrane folding and vesicle formation during macropinocytosis, thereby influencing the efficiency and regulation of this cellular uptake mechanism. Thus, we further monitored actin rearrangement during RGNNV infection in hMMES1 cells. hMMES1 cells were stained with DAPI and iFluorTM-488 conjugated phalloidin at 4 hpi, specifically binding to the polymerized form of actin (F-actin). Intriguingly, RGNNV infection led to depolymerization and changes in actin distribution. The number of F-actin filaments decreased, and actin-driven membrane protrusions co-localized with virions were observed on the cell surface of infected cells, absent in mock-infected control cells (Fig. 8M). These results suggest that MmRac1 and MmCdc42 facilitate RGNNV internalization by driving macropinocytosis through actin cytoskeletal dynamics.

Discussion

NNV, an important fish virus, enters host cells by utilizing a range of host factors that act as receptors and facilitate the process of endocytosis via an orchestrated mechanism. Three host factors, HSP90ab1,HSC70 and Nectin1, have been identified as entry receptors of NNV (Chang and Chi, 2015; Zhang et al., 2020, n.d.), however, disrupting their interaction with cells does only partially hinder viral infection, suggesting that NNV likely utilizes additional, yet unidentified host receptors or co-receptors. To establish infection, NNV utilized receptor-mediated endocytosis to induce internalization

of the virus/receptor complex, primarily including CME and macropinocytosis (Liu et al., 2005). Although previous studies demonstrate that HSP90ab1 and HSC70 are responsible for NNV internalization via CME, the receptor and the molecular mechanisms leading to NNV entry into cells via macropinocytosis remain to be determined. In this study, we found that NNV gain entry into host cells via the interaction between CP and its novel receptor MmMYL3. Subsequently, MmMYL3 engages with IGF1R, leading to the activation of the Rac1/Cdc42 pathway, which induces actin rearrangement and facilitates NNV macropinocytosis (Fig. 9).

Numerous data indicate the significance of myosin light chains in the functionality of both cardiac and skeletal muscles. However, little is known about the function of myosin light chains during virus infection (Kamm and Stull, 2011; Sheikh et al., 2016; Yu et al., 2016). Here, we provide several lines of evidence showing that MmMYL3 acts as a novel receptor of NNV. First, ectopic expression of MmMYL3 facilitates internalization of RGNNV, which is mediated by the interaction between the EF-hand2 domain of MmMYL3 and the arm and S domain of CP. Considering that our previous study had reported that MmHSP90ab1, a known NNV receptor, interacted with the linker region of CP (Zhang et al., 2020). Thus, we speculated that NNV might have the ability to utilize multiple receptors simultaneously for cell infection through these receptors binding to the different domains of CP. Furthermore, interference with the MmMYL3 and CP interaction with abs against MYL3, MmMYL3 fusion protein and CP arm domain peptides significantly block NNV entry, providing a potential antiviral strategy against NNV infection. In addition to these *in vitro* findings, our *in vivo* experiments further confirm the physiological relevance of MmMYL3 in viral pathogenesis and highlight its potential as a therapeutic target in aquaculture. More importantly, virus-resistant HEK293T cells are rendered susceptible to RGNNV infection by overexpression of MmMYL3 alone. The development of MmMYL3 overexpressing HEK293T cells model offers a valuable platform for investigating viral infection mechanisms and conducting drug screening studies. All these results suggested that MmMYL3 is a novel receptor that mediates NNV entry. We also found that the interaction of MYL3 with CP was conserved across NNV sensitive fish. Interestingly, NNV exhibits a broad species

tropism, capable of infecting diverse cell lines and various animal species examined thus far (Munday et al., 2002). This phenomenon may be attributed in part to the robust conservation of MYL3. To the best of our knowledge, this is the first study to provide evidence that MYL3 functions as a functional entry receptor for virus.

Nodaviridae viruses are divided into two genera: *Alphanodavirus* and *Betanodavirus*. *Alphanodaviruses* typically infect insects, whereas *Betanodaviruses* primarily infect fish (Yong et al., 2017). In recent years, a novel *Alphanodavirus*, provisionally named covert mortality nodavirus (CMNV), has emerged, causing viral covert mortality disease in shrimp and also affecting farmed marine fish (Wang et al., 2021; Zhang et al., 2014). Given the susceptibility of marine fish to CMNV, we investigated the possibility that both *Alphanodavirus* and *Betanodavirus* utilize MYL3 as a common receptor for cellular entry. Sequence comparison results revealed a low homology between the CP protein sequences of CMNV and RGNNV. Additionally, our data indicated that the CP of CMNV did not interact with MmMYL3 (data not shown). These findings suggest that MmMYL3 may function as a receptor specific to *Betanodavirus*, rather than being a common receptor for both viral genera.

Previous reports have highlighted the dependence of the NNV entry process on both CME and macropinocytosis pathways (Liu et al., 2005). We had demonstrated NNV can use MmHSP90ab1 and MmHSC70 to enter cells via CME pathway (Chang and Chi, 2015; Zhang et al., 2020). In contrast to these receptors, our findings revealed that MmMYL3 promotes NNV internalization via macropinocytosis. Macropinocytosis, characterized as a transient, growth factor-induced, actin-dependent endocytic pathway, facilitates the internalization of fluid and membrane into large vacuole (Mercer and Helenius, 2009). Mounting evidence underscores its pivotal role as an endocytic route exploited by numerous viruses for invading host cell (Huang et al., 2008; Locker et al., 2000; Mercer and Helenius, 2008). Upon binding to the cell membrane, viruses trigger the activation of RTKs or other signaling molecules such as Rac1, Cdc42, and Pak1, initiating intricate intracellular signaling cascades that lead to alterations in actin filament dynamics and induction of plasma membrane ruffling (Bar-Sagi and Feramisco, 1986;

Bar-Sagi et al., 1987; Letizia Lanzetti, 2004). RTKs, well-known upstream regulatory factors of macropinocytosis, are involved in the entry process of various viruses (Amyere et al., 2000; Nicola et al., 2005). To evaluate the significance of RTKs in NNV entry, we conducted a screening of small molecules targeting the activation of specific RTKs. Our findings revealed that AZD-3463 and Picropodophyllin, two inhibitors of IGF1R, could impede MmMYL3-mediated RGNNV entry. IGF1R is a transmembrane RTK involved in mediating cellular responses to IGFs and plays a significant role in cellular processes such as growth, proliferation, and survival (Hakuno and Takahashi, 2018; Pellegrino et al., 2024). Recent studies have revealed an intriguing connection between IGF1R signaling and viral entry mechanisms, particularly through macropinocytosis (Józefiak et al., 2021; Stewart et al., 2021). Our findings revealed direct binding between MmMYL3 and MmIGF1R, indicating that MmMYL3 might participated in the macropinocytosis-mediated NNV entry through its interaction with MmIGF1R. Previous study had identified IGF1R as an entry receptor for respiratory syncytial virus (Griffiths et al., 2020). Consider the conservation of IGF1R, we investigated whether it could serve as a potential receptor for NNV. However, our analysis indicated that MmIGF1R did not directly bind to CP, indicating that MmIGF1R might not be the receptor for NNV.

To further explore how MmIGF1R promotes macropinocytosis and NNV internalization, we investigate the effect of MmIGF1R downstream signaling on NNV infection. IGF1R can activate GTPases, such as Cdc42 and Rac1, leading to rapid actin reorganization and membrane ruffling, key processes in initiating macropinocytosis (Dam et al., 2017; Manara et al., 2016). Increasing evidence has demonstrate that Cdc42 and Rac1 are essential for various virus entry (Lu et al., 2023; Swaine and Dittmar, 2015; Zhang et al., 2021). We found that both MmRac1 and MmCdc42 interact with the intracellular domain of MmIGF1R, and inhibition of MmRac1 and MmCdc42 significantly impaired RGNNV entry. Conversely, overexpression of MmRac1 or MmCdc42 enhanced NNV internalization. Actin filaments play a central role in driving the membrane dynamics necessary for the formation and internalization of macropinosomes during macropinocytosis. We found that there was a notable

reorganization of F-actin filaments, accompanied by the presence of actin-driven membrane protrusions that co-localized with virions on the surface of RGNNV infected cells. All these results indicated that cytosis MmIGF1R regulate Rac1/Cdc42 signaling to promotes macropinocytosis during NNV infection. While previous studies have suggested that NNV enters host cells via macropinocytosis, our study was the first to provide a detailed mechanism understanding of this process.

Our study provides strong evidence that MmMYL3 serves as a receptor for RGNNV *in vitro*, however, one limitation of our research is the lack of *in vivo* experiments using MmMYL3 knockout marine medaka. Conducting these knockout studies would further validate the role of MmMYL3 in NNV infection in a whole organism context. Unlike well-established model organisms like zebrafish or mice, gene editing in marine medaka is fraught with difficulties, including technical complexity, precise embryo microinjection, and the potential for off-target effects with CRISPR/Cas9 technology. The process is time-consuming, requiring multiple breeding generations and thorough molecular screening to establish homozygous knockout lines. Future research aimed at developing these knockout models will greatly benefit from advances in gene editing technologies and standardized protocols tailored to marine medaka.

Overall, MmMYL3 was identified as a novel functional receptor for RGNNV. Moreover, MmMYL3 was involved in and facilitated RGNNV internalization through the macropinocytosis pathway via the IGF1R-Rac1/Cdc42 axis. Our findings shed new light on the molecular mechanism of RGNNV entry and provide a new perspective for the development of antiviral therapies.

Materials and methods

Cell Culture

hMMES1 cell line, derived from marine medaka embryo blastocysts, was demonstrated to be susceptible to RGNNV. hMMES1 cells were cultivated in ESM4 medium at 28˚C as previously described (Zhang et al., 2020). HEK293T cells were cultured in DMEM

medium supplemented with 10% heat-inactivated fetal bovine serum (FBS, Yeasen, China) under standard conditions of 37˚C with 5% CO_2.

Virus generation

The RGNNV strain, originally isolated from afflicted sea perch larvae and juveniles in Guangdong Province, China, was propagated in LJB cells (Jia et al., 2015; Le et al., 2017) and preserved as viral stocks at −80˚C for use.

Cell transfection and NNV infection

hMMES1 in six-well plates (1×10^6 cells/well) were transfected with different plasmids using Lipofectamine 8000 (Beyotime) following the manufacturer's instructions. At 24 h post-transfection, the cells were infected with RGNNV at a multiplicity of infection (MOI) of 1 for the indicated hours and examined by quantitative reverse transcription-PCR (qRT-PCR).

To detect the viral titers, hMMES1 cells transfected with pCMV-Flag-MmMYL3 or MmMYL3-siRNA were infected with RGNNV (MOI=1) at 28˚C for 4 h, the culture medium was removed and incubated with fresh medium for 48 h, then the supernatant was collected for viral titer assay as described previously (W. Zhang et al., 2022).

RNA interference

Small interfering RNAs (siRNAs) targeting MmMYL3 (siMmMYL3) were synthesized by the Ribobio company (Guangzhou, China), including siRNA-1 (5′-GGCTCAACTTTGACGCCTT-3′), siRNA-2(5′-CTGAGCTGCGAATTGTGCT-3′), siRNA-3 (5′-GCTGTAGCTTGCCTACAGA-3′), and control siRNA (NC) (5′-UUCUCCGAACGUGUCACGUTT-3′). siRNAs targeting MmIGF1R (siMmIGF1R) were siRNA-4 (5′-GCACAACTTGACAATCCGA-3′), siRNA-5 (5′-CGTCACATCAAGTTATACA-3′), siRNA-6 (5′-GCAATCTGACGTACTACCT-3′). Transfection of siRNAs was conducted using a mixture of three different siRNAs at concentrations of 50 or 100 nM as described previously (W. Zhang et al., 2022).

qRT-PCR

Total RNA of cultured cells was extracted with TRIzol reagent (Invitrogen, CA, USA) according to the manufacturer's instructions and was further reverse transcribed into cDNA through the GoScript^{TM} Reverse Transcription Mix (Promega, Madison, USA). A LightCycler 480 II (Roche Applied Science, Germany) and qPCR SYBR Green Master Mix (Yeasen) were used for qRT-PCR analysis by using gene-specific primers (Table S1). mRNA relative expression levels were evaluated from triplicate experiments and normalized to marine medaka *β-actin*. The relative fold induction of genes was calculated using the threshold cycle ($2^{-\Delta\Delta CT}$) method and presented as mean ± standard deviation (SD).

Western blot and Co-IP

The cells were lysed with lysate buffer (Beyotime) and boiled for 10 min with 1% SDS for SDS-PAGE separation. The proteins were transferred onto polyvinylidene difluoride (PVDF) membranes (Millipore, USA) and then blocked with 5% nonfat dried milk for 1 h at room temperature (RT), followed by incubation with primary antibodies at 4°C overnight, including anti-Flag (1:4,000), anti-Myc (1:4,000), anti-GFP (1:4,000), anti-MYL3 (1:1,000) and anti-actin (1:4,000) antibodies. Subsequently, membranes were further probed with goat anti-rabbit or anti-mouse IgG (H+L) highly cross-adsorbed secondary antibodies (1:1,000) for 1 h at RT and analyzed using enhanced chemiluminescence (ECL) immunoblotting detection reagents (Millipore, USA) on a chemiluminescence instrument (Sage Creation, China).

For the Co-IP assay, cell extracts were incubated with anti-Flag/Myc/GFP magnetic beads at 4°C overnight. After incubation, the beads were washed five times with lysis buffer and eluted with 1% SDS buffer for boiling. The eluted samples were subjected to Western blot analysis.

Protein purification and pulldown assays

The pET-GST-MmMYL3 and empty pET-GST were transformed into *Escherichia coli* BL21 (DE3), separately. Bacteria were grown to an OD600 of 0.8–1.0 and then induced with 0.5 mM IPTG for 12 h at 20°C in a shaking incubator. MYL3-GST protein and GST protein were purified using the GST spin purification kit (Beyotime) according to the manufacturer's instruction. Briefly, the bacterial solution was collected and washed three times with PBS. Lysozyme was added to a final concentration of 1 mg/ml, and placed on ice for 30 min, then centrifuged at 4°C for 10 min. The supernatant was purified using the BeyoGold™ GST-tag Purification Resin as described previously (Lv et al., 2022). Finally, the protein was eluted from the column. The purified protein was stained with Coomassie brilliant blue.

GST-Tag magnetic beads were first mixed with the GST-fused MmMYL3s for 4 h at RT. Then, the beads were incubated with protein lysates from HEK293T cells transfected with pCMV-Flag-CP or p-EGFP-MmIGF1R at 4°C overnight and finally analyzed by Western blotting. For the pulldown assay between MmMYL3 and RGNNV, the beads incubated with GST-fused proteins were mixed with RGNNV viral stock (500 μL) at 4°C for 4 h. Then, the beads were subjected to SDS-PAGE.

Surface Plasmon Resonance (SPR) analysis

Biacore™ T200 (GE, USA) was used to analyze the interaction between MmMYL3 and the CP protein. Briefly, purified CP protein was first diluted (20 μg/mL) with 200 μL of sodium acetate buffer (10 mM, pH 4.0) and then flowed across the activated surface of a CM5 sensor chip (BR100012, GE, USA) at a flow rate of 10 μL/min, reaching a resonance unit (RU) of ~2□500. The remaining activated sites on the chip were blocked with 75 μL of ethanolamine (1 M, pH 8.5). Serial concentrations of MmMYL3 protein (5, 10, 20, 40, 80 μM) in PBS buffer (0.01 M, pH 7.4) were applied to analyze their interactions with immobilized CP at a flow rate of 10 μL/min. The K_D for binding and Ka and Kd rate constants were determined using the BIA evaluation program (GE, USA).

Proteinase K protection assay

The proteinase K protection assay was performed as described previously with some modification (Zhang et al., 2020). Briefly, hMMES1 and HEK293T cells were seeded into 6-well culture plates and transfected with pCMV-Flag-MmMYL3 plasmids for 24 h. After washed with PBS for three times, one group of cells were treated with 10 μg/ml of proteinase K for 30 min in an ice water bath, another group was added with the same volume of PBS, the reaction was stopped by addition of PMSF. Cells were then lysed with lysis buffer on ice for 30 min, the whole cell lysates were resuspended in SDS loading buffer and analyzed by Western blot using anti-Flag or anti-Actin abs.

Flow cytometry

Cells were seeded on six-well plates overnight and scraped off the plate and washed with PBS. For detection of surface expression of MmMYL3, cells were suspended with 200 μL PBS and incubated with anti-Alexa Flour 488-Myc antibody at 2 μg/mL on ice for 2 h. Cells were then washed with PBS and analyzed by flow cytometry.

Transmission electron microscopy (TEM)

Cell samples and ultrathin sections for TEM were prepared as described previously (Dong et al., 2014). Cells were collected and fixed at 4˚C for 24 h with 2.5% glutaraldehyde in 0.1 M PBS (pH 7.4) and 2.0% osmium tetroxide in 0.1 M PBS in turn, ultrathin sections were observed under a Philips CM10 transmission electron microscope.

Immunofluorescence assays

To examine the localization of MmMYL3 proteins on cells, IF assays were performed as described previously with some modification (Jia et al., 2013). Briefly, hMMES1 and HEK293T cells were seeded into 24-well culture plates on glass coverslips and were separately transfected with pCMV-Myc and pCMV-Myc-MmMYL3 plasmids, respectively. After transfection for 24 h, cells were washed with PBS, fixed with 4% paraformaldehyde for 10 min at RT. One group was treated with 0.2% Triton X-100 for membrane permeabilization, and the other was not. After being washed three times with PBS, cells were blocked with PBS containing 5% bovine serum albumin at RT for 1 h

and then reacted with anti-Myc abs (1:400) at 4˚C overnight. Anti-Actin abs were used as negative control. After three times wash with PBS, cells were incubated with Alexa Fluor 555 goat anti-mouse IgG (Invitrogen) at a dilution of 1:400 for 1 h at RT. Cells were then washed with PBS and stained the cell nuclei with DAPI for 10 min. The coverslips were washed with PBS and observed under an SP8 Leica laser confocal microscopy imaging system (SP8, Leica, Germany).

For assessment of the colocalization, HEK293T cells plated on coverslips in 24-well plates were transfected with different plasmids. After transfection for 24 h, cells were washed with PBS then fixed and permeabilized as described above. The cells were incubated with primary antibodies at 4°C overnight, including anti-Flag (1:400) and anti-Myc (1:400) antibodies, followed by incubation with Alexa Fluor 555- or 488-conjugated secondary antibodies against mouse or rabbit IgG (1:400). Finally, cells were observed under a confocal microscope.

For cell membrane staining, hMMES1 cells were labeled with PKH 26 (red fluorescent, MCE). PKH 26 was dissolved in DMSO to obtain 1 mM stock solution of PKH 26. The stock solution was diluted with PBS at 1:100 to obtain the 10 μM working solution. hMMES1 cells were incubated with the working solution at 28°C for 30 min. After the incubation, the cells were washed using PBS to remove unlabeled cells and detected as described above.

For RGNNV entry detection, HEK293T were transfected with pCMV-Flag-MmMYL3 for 24h, and then infected with RGNNV (MOI=5). After infection for 24 h, the cells were detected with IF assays, cells were incubated with rabbit anti-CP abs and detected as described above.

To observe actin cytoskeleton dynamics after virus infection, hMMES1 cells were exposed to RGNNV (MOI=1) at 4°C and incubated for 4 h. The temperature shift was performed after washing with PBS by using prewarmed (28°C) serum-free medium for 30 min. Afterwards, cells were fixed with 4% paraformaldehyde and permeabilized with 0.2% Triton X-100 at room temperature. The cells were incubated with anti-CP antibody

(1:200) at 4°C overnight. iFluorTM 488 phalloidin and DAPI were used to stain actin filaments and nuclei of cells, respectively(Delpeut et al., 2017).

Dextran uptake assay for macropinocytosis

Following a published procedure (Y. Y. Zhang et al., 2022), hMMES1 cells on cover slips were treated with indicated chemical compound. After treatment, the cells were serum-starved for 16 h. The cells were infected with RGNNV (MOI=1) in media containing Alexa Fluor 647-conjugated dextran (10,000 MW), incubated for 4 h at 28˚C, and washed and fixed for 16 h with 4% PFA at 4˚C. For co-localization experiments, the cells also were stained for MmMYL3 and CP using specific antibodies as described above. Samples were viewed and evaluated by confocal microscopy.

Blocking assays

MYL3-GST protein was affinity-purified as described above. RGNNV (10^3 $TCID_{50}$) were incubated with different concentrations (100 or 500 ng) of recombinant MYL3-GST protein for 4 h at 4˚C. Then, hMMES1 cells were incubated with virus and protein mixtures for 4 h at 4˚C. Similarly, cells were treated with 10^3 $TCID_{50}$ of RGNNV preincubated with BSA (500 ng) as a control. Then, cells were harvested, CP and RDRP mRNA were measured as described above.

hMMES1 cells were pre-seeded in 12-well plates overnight. Due to the unavailability of anti-MmMYL3 abs and the high homogeneity of MYL3 at the N-terminus domain between human and fish, cells were incubated with anti-human MYL3 abs (1:50) (Abcam) for 4 h at 28˚C. After washed with fresh media, cells were infected with RGNNV (MOI=1) at 4˚C for 2 and 4 h, respectively. As a control, hMMES1 cells were in parallel pretreated with normal rabbit IgG. Cells were then washed three times with PBS to remove free virus particles and harvested for total RNA extraction and qRT-PCR detection of RGNNV CP and RDRP.

To evaluate the implication of arm (short peptide of CP, RTDAPVSKASTVTGFGRG, Sangon, Shanghai) on RGNNV entry, hMMES1 cells

were pretreated with different doses (0, 5, 10, 20, 40 μM) of these samples for 4 h. Then, the virus (MOI=1) was subsequently added to allow infection for 4 h. The virus-protein mixture was removed, and cells were further cultured with fresh protein-containing medium for 24 h. The qRT-PCR protocols were performed as described above.

Inhibitor treatment assay

Cells were treated with various inhibitors to investigate the endocytosis pathway utilized by RGNNV for cell entry. hMMES1 cells or MmMYL3-overexpressing hMMES1 cells were treated with different inhibitors for 4 h, then infected with RGNNV (MOI=1) for 4 h at 28˚C. Next, the cells were washed with PBS for three times to remove any unbound viruses. DMSO was used as control. Total RNA of cells was extracted for qRT-PCR detection.

RGNNV infection of marine medaka

Marine medaka were divided into two groups: the MmMYL3 group and the GST group (n = 30 per group). Correspondingly, RGNNV (100 $TCID_{50}$) was incubated with purified GST-tagged MmMYL3 recombinant protein or GST protein for 4 h at 4˚C, then the mixtures were injected into two groups of marine medaka separately. The negative control group of fishes were injected with the same volume of PBS. The survival rate of each group was recorded every day by counting the numbers of dead fish. The log-rank test method was used to analyze the differences between groups. Marine medaka were necropsied and the eyes and brains were collected at day 5 post infection for further measurement of viral loads and pathological analysis. **, $P < 0.01$. The animal study was reviewed and approved by the Ethics Committee of Sun Yat-Sen University (Approval No. SYSU-IACUC-2023-000168).

Quantification and statistical analysis

Data were collected from three independent experiments, analyzed with SPSS version 20.0, and presented as the means ± SDs. Student's *t* test or one-way analysis of variance (ANOVA) was used for the statistical comparisons between two groups or

multiple groups, respectively. *P* value <0.05 was considered to indicate a statistically significant difference; *P* value < 0.01 was considered to indicate a highly significant difference.

Supplementary Materials

Materials and Methods

Fig.S1. Expression analysis of MmMYL3 in hMMES1 cells at 2, 4, 24 and 48 h post RGNNV infection.

Fig.S2. Recombinant expression and purification of MmMYL3-GST and GST.

Fig.S3. MYL3 antibody validation.

Table S1. Primer sequences used by application.

Acknowledgments

Funding: This work was supported by the National Natural Science Foundation of China (32173001), Natural Science Foundation of Guangxi Province (2021GXNSFDA075015), Scientific and Technological Planning Project of Guangzhou City (2023B03J1267), Natural Science Foundation of Guangdong Province (2023B1515120074; 2024A1515010880) and Open Project Program of State Key Laboratory of Biocontrol (2023SKLBC-KF03).

Author contributions: Conceptualization: M.Y and K.J.; Methodology: L.Y., W.Z. and X.Y.; Investigation: L.Y. and W.Z.; Supervision: K.J., and M.Y; Funding acquisition: K.J., and M.Y; Writing – Original Draft: L.Y., W.Z., K.J., and M.Y.

Competing interests: The authors declare no competing interest.

Data and materials availability: All data are available in the main text or the supplementary materials.

References

Amyere M, Payrastre B, Krause U, Van Der Smissen P, Veithen A, Courtoy PJ. 2000. Constitutive macropinocytosis in oncogene-transformed fibroblasts depends on sequential permanent activation of phosphoinositide 3-kinase and phospholipase C. *Mol Biol Cell* **11**:3453–3467. doi:10.1091/mbc.11.10.3453

Arii J, Goto H, Suenaga T, Oyama M, Kozuka-Hata H, Imai T, Minowa A, Akashi H, Arase H, Kawaoka Y, Kawaguchi Y. 2010. Non-muscle myosin IIA is a functional entry receptor for herpes simplex virus-1. *Nature* **467**:859–862. doi:10.1038/nature09420

Bandín I, Souto S. 2020. Betanodavirus and VER Disease: A 30-year. *Pathogens* **9**:1–46.

Banerjee I, Miyake Y, Philip Nobs S, Schneider C, Horvath P, Kopf M, Matthias P, Helenius A, Yamauchi Y. 2014. Influenza A virus uses the aggresome processing machinery for host cell entry. *Science (80-)* **346**:473–477. doi:10.1126/science.1257037

Bar-Sagi D, Feramisco JR. 1986. Induction of membrane ruffling and fluid-phase pinocytosis in quiescent fibroblasts by ras proteins. *Science (80-)* **233**:1061–1068. doi:10.1126/science.3090687

Bar□Sagi D, McCormick F, Milley RJ, Feramisco JR. 1987. Inhibition of cell surface ruffling and fluid□phase pinocytosis by microinjection of anti□ras antibodies into living cells. *J Cell Physiol* **133**:69–73. doi:10.1002/jcp.1041330414

Chang J-S, Chi S-C. 2015. GHSC70 Is Involved in the Cellular Entry of Nervous Necrosis Virus. *J Virol* **89**:61–70. doi:10.1128/jvi.02523-14

Costa JZ, Thompson KD. 2016. Understanding the interaction between Betanodavirus and its host for the development of prophylactic measures for viral encephalopathy and retinopathy. *Fish Shellfish Immunol* **53**:35–49. doi:10.1016/j.fsi.2016.03.033

Dam DHM, Wang XQ, Sheu S, Vijay M, Shipp D, Miller L, Paller AS. 2017. Ganglioside GM3 Mediates Glucose-Induced Suppression of IGF-1 Receptor–Rac1 Activation to Inhibit Keratinocyte Motility. *J Invest Dermatol* **137**:440–448. doi:10.1016/j.jid.2016.09.028

Delpeut S, Sisson G, Black KM, Richardson CD. 2017. Measles Virus Enters Breast and Colon Cancer Cell Lines through a PVRL4-Mediated Macropinocytosis Pathway. *J Virol* **91**. doi:10.1128/jvi.02191-16

Dong S, Kang M, Wu X, Ye T. 2014. Development of a promising fish model (Oryzias melastigma) for assessing multiple responses to stresses in the marine environment. *Biomed Res Int* **2014**. doi:10.1155/2014/563131

Foth BJ, Goedecke MC, Soldati D. 2006. New insights into myosin evolution and classification. *Proc Natl Acad Sci U S A* **103**:3681–3686. doi:10.1073/pnas.0506307103

Griffiths CD, Bilawchuk LM, McDonough JE, Jamieson KC, Elawar F, Cen Y, Duan W, Lin C, Song H, Casanova JL, Ogg S, Jensen LD, Thienpont B, Kumar A, Hobman TC, Proud D, Moraes TJ, Marchant DJ. 2020. IGF1R is an entry receptor for respiratory syncytial virus. *Nature* **583**:615–619. doi:10.1038/s41586-020-2369-7

Grove J, Marsh M. 2011. The cell biology of receptor-mediated virus entry. *J Cell Biol* **195**:1071–1082. doi:10.1083/jcb.201108131

Hakuno F, Takahashi SI. 2018. 40 years of IGF1: IGF1 receptor signaling pathways. *J Mol Endocrinol* **61**:T69–T86. doi:10.1530/JME-17-0311

He J, Qiu Y, Tan L, Duan D, Yuan X, Yang L, Wang A. 2022. Understanding the key functions of Myosins in viral infection. *Biochem Soc Trans* **50**:597–607. doi:10.1042/BST20211239

Huang C-Y, Lu T-Y, Bair C-H, Chang Y-S, Jwo J-K, Chang W. 2008. A Novel Cellular Protein, VPEF, Facilitates Vaccinia Virus Penetration into HeLa Cells through Fluid Phase Endocytosis. *J Virol* **82**:7988–7999. doi:10.1128/jvi.00894-08

Huang PY, Hsiao HC, Wang SW, Lo SF, Lu MW, Chen LL. 2020. Screening for the Proteins That Can Interact with Grouper Nervous Necrosis Virus Capsid Protein. *Viruses* **12**:1–20. doi:10.3390/v12090985

Ingles J, Doolan A, Chiu C, Seidman J, Seidman C, Semsarian C. 2005. Compound and double mutations in patients with hypertrophic cardiomyopathy: implications for genetic testing and counselling. *J Med Genet* **42**:2–7. doi:10.1136/jmg.2005.033886

Jia K-T, Wu Y-Y, Liu Z-Y, Mi S, Zheng Y-W, He J, Weng S-P, Li SC, He J-G, Guo C-J. 2013. Mandarin Fish Caveolin 1 Interaction with Major Capsid Protein of Infectious Spleen and Kidney Necrosis Virus and Its Role in Early Stages of Infection. *J Virol* **87**:3027–3038. doi:10.1128/jvi.00552-12

Jia P, Jia KT, Yi MS. 2015. Complete genome sequence of a fish nervous necrosis virus isolated from sea perch (Lateolabrax japonicus) in China. *Genome Announc* **3**:455643. doi:10.1128/genomeA.00048-15

Józefiak A, Larska M, Pomorska-Mól M, Ruszkowski JJ. 2021. The igf-1 signaling pathway in viral infections. *Viruses* **13**:1–11. doi:10.3390/v13081488

Kamm KE, Stull JT. 2011. Signaling to myosin regulatory light chain in sarcomeres. *J Biol Chem* **286**:9941–9947. doi:10.1074/jbc.R110.198697

Le Y, Li Y, Jin Y, Jia P, Jia K, Yi M. 2017. Establishment and characterization of a brain cell line from sea perch, Lateolabrax japonicus. *Vitr Cell Dev Biol - Anim* **53**:834–840. doi:10.1007/s11626-017-0185-7

Letizia Lanzetti APLAS& PPDF. 2004. Rab5 is a signalling GTPases. *Nature* **429**:309–314.

Li L, Xue B, Sun W, Gu G, Hou G, Zhang L, Wu C, Zhao Q, Zhang Y, Zhang G, Hiscox JA, Nan Y, Zhou EM. 2018. Recombinant MYH9 protein C-terminal domain blocks porcine reproductive and respiratory syndrome virus internalization by direct interaction with viral glycoprotein 5. *Antiviral Res* **156**:10–20. doi:10.1016/j.antiviral.2018.06.001

Liu W, Hsu CH, Hong YR, Wu SC, Wang CH, Wu YM, Chao C Ben, Lin CS. 2005. Early endocytosis pathways in SSN-1 cells infected by dragon grouper nervous necrosis virus. *J Gen Virol* **86**:2553–2561. doi:10.1099/vir.0.81021-0

Locker JK, Kuehn A, Schleich S, Rutter G, Hohenberg H, Wepf R, Griffiths G. 2000. Entry of the two infectious forms of vaccinia virus at the plasma membane is signaling-dependent for the IMV but not the EEV. *Mol Biol Cell* **11**:2497–2511. doi:10.1091/mbc.11.7.2497

Lu ZZ, Sun C, Zhang X, Peng Y, Wang Y, Zeng Y, Zhu N, Yuan Y, Zeng MS. 2023. Neuropilin 1 is an entry receptor for KSHV infection of mesenchymal stem cell through TGFBR1/2-mediated macropinocytosis. *Sci Adv* **9**:1–17. doi:10.1126/sciadv.adg1778

Lv W, Jiang W, Luo H, Tong Q, Niu X, Liu X, Miao Y, Wang Jingnan, Guo Y, Li J, Zhan X, Hou Y, Peng Y, Wang Jian, Zhao S, Xu Z, Zuo B. 2022. Long noncoding RNA lncMREF promotes myogenic differentiation and muscle regeneration by interacting with the Smarca5/p300 complex. *Nucleic Acids Res* **50**:10733–10755. doi:10.1093/nar/gkac854

Manara MC, Terracciano M, Mancarella C, Sciandra M, Guerzoni C, Pasello M, Grilli A, Zini N, Picci P, Colombo MP, Morrione A, Scotlandi K. 2016. CD99 triggering induces methuosis of Ewing sarcoma cells through IGF-1R/RAS/Rac1 signaling. *Oncotarget* **7**:79925–79942. doi:10.18632/oncotarget.13160

Marsh M, Helenius A. 2006. Virus entry: Open sesame. *Cell* **124**:729–740. doi:10.1016/j.cell.2006.02.007

Mavilakandy A, Ahamed H. 2022. Mutation of the MYL3 gene in a patient with mid-ventricular obstructive hypertrophic cardiomyopathy. *BMJ Case Rep* **15**:1–5. doi:10.1136/bcr-2021-244573

Melissa S. Maginnis. 2018. Virus-Receptor Interactions:The Key to Cellular Invasion. *J Mol Biol* **430**:2590–2611.

Mercer J, Helenius A. 2009. Virus entry by macropinocytosis. *Nat Cell Biol* **11**:510–520. doi:10.1038/ncb0509-510

Mercer J, Helenius A. 2008. Vaccinia virus uses macropinocytosis and apoptotic mimicry to enter host cells. *Science (80-)* **320**:531–535. doi:10.1126/science.1155164

Mercer J, Schelhaas M, Helenius A. 2010. Virus entry by endocytosis. *Annu Rev Biochem* **79**:803–833. doi:10.1146/annurev-biochem-060208-104626

Mori KI, Nakai T, Muroga K, Arimoto M, Mushiake K, Furusawa I. 1992. Properties of a new virus belonging to nodaviridae found in larval striped jack (Pseudocaranx dentex) with nervous necrosis. *Virology* **187**:368–371. doi:10.1016/0042-6822(92)90329-N

Munday BL, Kwang J, Moody N. 2002. Review article Betanodavirus infections of teleost ® sh□: a review. *J Fish Dis* 127–142.

Nicola A V., Hou J, Major EO, Straus SE. 2005. Herpes Simplex Virus Type 1 Enters Human Epidermal Keratinocytes, but Not Neurons, via a pH-Dependent Endocytic Pathway. *J Virol* **79**:7609–7616. doi:10.1128/jvi.79.12.7609-7616.2005

Pellegrino M, Secli V, D'Amico S, Petrilli LL, Caforio M, Folgiero V, Tumino N, Vacca P, Vinci M, Fruci D, de Billy E. 2024. Manipulating the tumor immune microenvironment to improve cancer immunotherapy: IGF1R, a promising target. *Front Immunol* **15**:1–10. doi:10.3389/fimmu.2024.1356321

Sheikh F, Lyon RC, Chen J, Jolla L. 2016. HHS Public Access **569**:14–20. doi:10.1016/j.gene.2015.06.027.Functions

Stewart CM, Phan A, Bo Y, LeBlond ND, Smith TKT, Laroche G, Giguère PM, Fullerton MD, Pelchat M, Kobasa D, Côté M. 2021. Ebola virus triggers receptor tyrosine kinase-dependent signaling to promote the delivery of viral particles to entry-conducive intracellular compartments. *PLoS Pathog* **17**. doi:10.1371/JOURNAL.PPAT.1009275

Swaine T, Dittmar MT. 2015. CDC42 Use in viral cell entry processes by RNA viruses. *Viruses* **7**:6526–6536. doi:10.3390/v7122955

Wang C, Liu S, Tang KFJ, Zhang Q. 2021. Natural infection of covert mortality nodavirus affects Zebrafish (Danio rerio). *J Fish Dis* **44**:1315–1324. doi:10.1111/jfd.13390

Yong CY, Yeap SK, Omar AR, Tan WS. 2017. Advances in the study of nodavirus. *PeerJ* **2017**:1–31. doi:10.7717/peerj.3841

Yu H, Chakravorty S, Song W, Ferenczi MA. 2016. Phosphorylation of the regulatory light chain of myosin in striated muscle: methodological perspectives. *Eur Biophys J* **45**:779–805. doi:10.1007/s00249-016-1128-z

Zhang C, Wang J, Wang G, Ji Z, Hou L, Liu Z, Chao T. 2016. Molecular cloning and mRNA expression analysis of sheep MYL3 and MYL4 genes. *Gene* **577**:209–214. doi:10.1016/j.gene.2015.11.041

Zhang F, Liu Y, You Q, Yang E, Liu B, Wang H, Xu S, Nawaz W, Chen D, Wu Z. 2021. NSC23766 and Ehop016 suppress herpes simplex virus-1 replication by inhibiting Rac1 activity. *Biol Pharm Bull* **44**:1263–1271. doi:10.1248/bpb.b21-00054

Zhang Q, Liu Q, Liu Shuang, Yang H, Liu Sun, Zhu L, Yang B, Jin J, Ding L, Wang X, Liang Y, Wang Q, Huang J. 2014. A new nodavirus is associated with covert mortality disease of shrimp. *J Gen Virol* **95**:2700–2709. doi:10.1099/vir.0.070078-0

Zhang W, Jia K, Jia P, Xiang Y, Lu X, Liu W, Yi M. 2020. Marine medaka heat shock protein 90ab1 is a receptor for red-spotted grouper nervous necrosis virus and promotes virus internalization through clathrin-mediated endocytosis. *PLoS Pathog* **16**:1–21. doi:10.1371/journal.ppat.1008668

Zhang W, Weng J, Yao L, Jia P, Yi M, Jia K. 2022. Nectin4 antagonises type I interferon production by targeting TRAF3 for autophagic degradation and disrupting TRAF3-TBK1 complex formation. *Int J Biol Macromol* **218**:654–664. doi:10.1016/j.ijbiomac.2022.07.151

Zhang YY, Liang R, Wang SJ, Ye ZW, Wang TY, Chen M, Liu J, Na L, Yang YL, Yang YB, Yuan S, Yin X, Cai XH, Tang YD. 2022. SARS-CoV-2 hijacks macropinocytosis to facilitate its entry and promote viral spike–mediated cell-to-cell fusion. *J Biol Chem* **298**:102511. doi:10.1016/j.jbc.2022.102511

Zhang Z, Xing J, Tang X, Sheng X, Chi H, Zhan W. n.d. 2024. Nectin1 is a pivotal host factor involved in attachment and entry of red-spotted grouper nervous necrosis virus in the early stages of the viral life cycle. *J Virol.*

Figure Legends

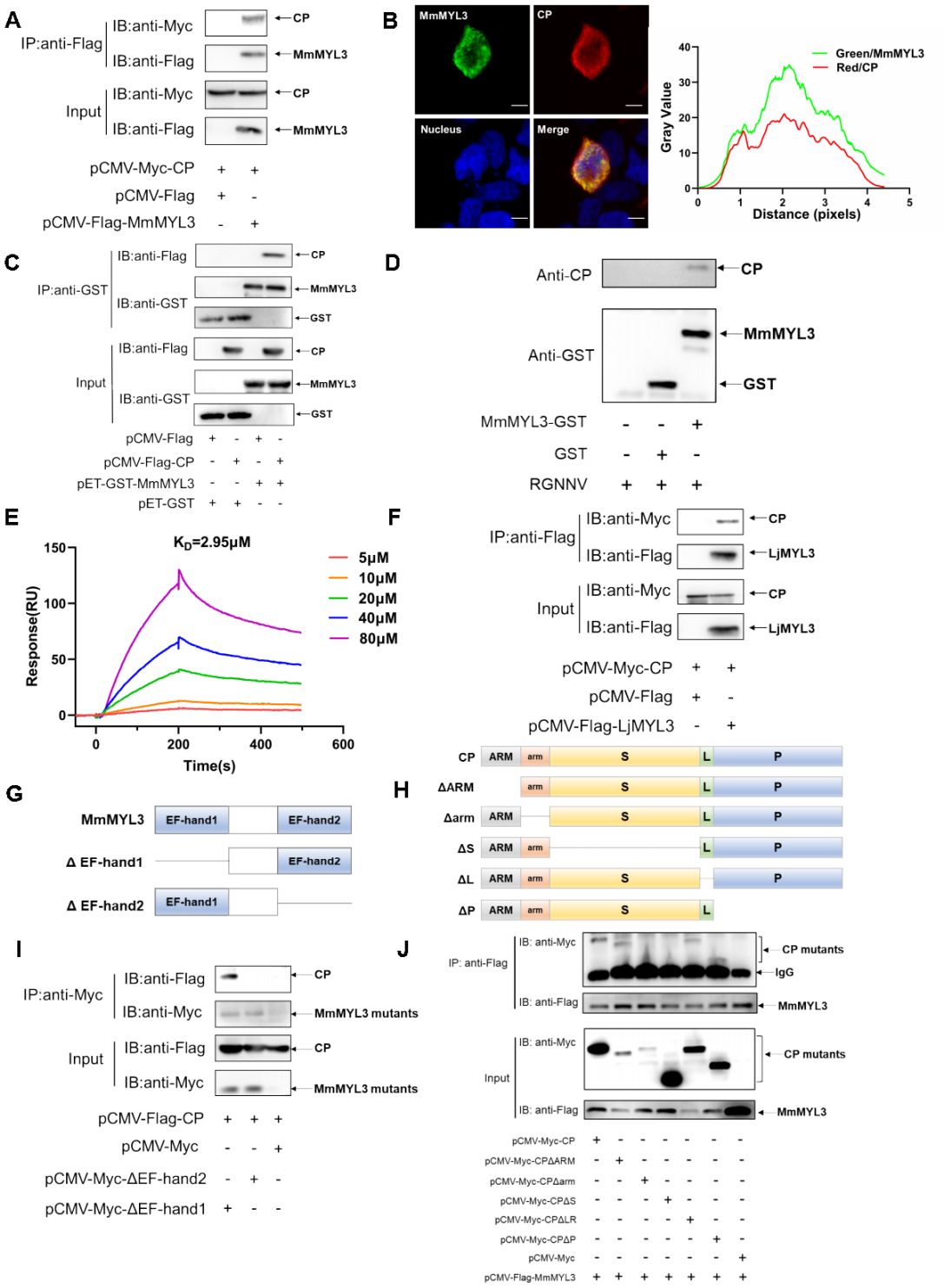

Fig.1. MmMYL3 interacts with CP. (A) Immunoprecipitation (IP) (with anti-Flag) and immunoblot analysis (with anti-Flag and anti-Myc) of HEK293 cells transfected with

plasmids encoding MmMYL3-Flag and CP-Myc for 48 h. (B) HEK293T cells were cotransfected with MmMYL3-Flag and CP-Myc plasmids. MmMYL3 (green) and CP (red) were detected by immunofluorescence staining with anti-Flag or anti-Myc abs, respectively. Nucleus were stained by DAPI, Bar = 10 μm. (C) The lysates of HEK293T cells transfected with indicated plasmids were pulled down with purified MmMYL3-GST or GST proteins followed by immunoblotting with anti-GST and anti-Flag abs. (D) Pull-down of RGNNV virions by MmMYL3-GST or GST proteins. RGNNV, purified proteins and magnetic streptavidin beads were co-incubated as indicated. Pull-down was performed with a magnet and the pellet was subjected to Western blot analysis. (E) SPR analysis of MmMYL3-CP protein interaction. 1:1 binding model was used to calculate the K_D. (F) Plasmids carrying MYL3 from sea perch (LjMYL3) were transfected into HEK293T cells, together with CP-Myc plasmid. At 48 h posttransfection, the cell lysates were subjected to coimmunoprecipitation analysis with anti-Flag magnetic beads as indicated. (G) Schematic diagram of MmMYL3 and its truncated mutants. (H) Schematic diagram of CP and its truncated mutants. (I) Immunoprecipitation (IP) (with anti-Myc) and immunoblot analysis (with anti-Flag and anti-Myc) of HEK293 cells transfected with plasmids encoding CP-Flag and Myc-tagged full-length MmMYL3 or its truncated mutants for 48 h. (J) HEK293T cells were cotransfected with MmMYL3-Flag and different Myc-tagged CP mutants for 48 h. Co-IP assays were performed as described above.

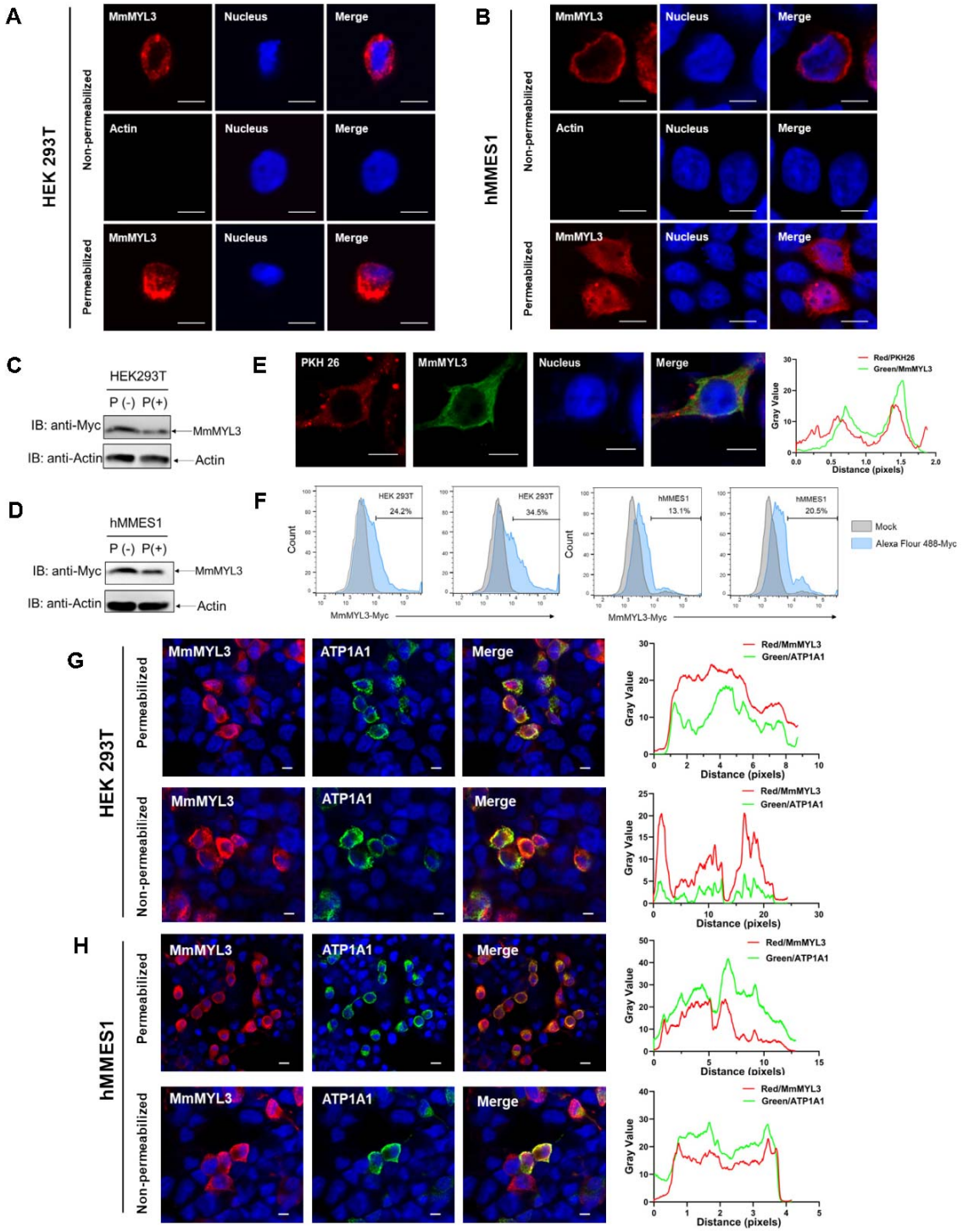

Fig.2. Surface localization of MmMYL3 in HEK293T and hMMES1 cells. (A and B) HEK293T (A) or hMMES1 (B) cells transfected with MmMYL3-Myc plasmids were fixed with formalin, treated with Triton X-100 or not and immunostained with anti-Myc

abs or anti-Actin abs, respectively. Cell nuclei were stained with DAPI. Bar = 10 μm. (C and D) HEK293T and hMMES1 cells transfected with MmMYL3-Myc plasmid were treated with proteinase K (P+) or without proteinase K (P-) and harvested for a Western blot analysis using anti-Myc and anti-Actin abs. (E) hMMES1 cells transfected with MmMYL3-Myc plasmid were labeled with PKH 26 (red) and stained with anti-Myc abs (green). Nucleus were stained by DAPI, Bar = 10 μm. (F) HEK293T and hMMES1 cells transfected with Myc-MmMYL3 were stained with Alexa Fluor 488-conjugated anti-Myc abs. Surface expression of MmMYL3 was analyzed by flow cytometry. (G and H) HEK293T or hMMES1 cells were cotransfected with MmMYL3-Myc and ATP1A1-Flag plasmids. MmMYL3 (red) and ATP1A1 (green) were detected by immunofluorescence staining with anti-Myc or anti-Flag abs in permeabilized or non-permeabilized conditions. Nucleus were stained by DAPI, Bar = 10 μm.

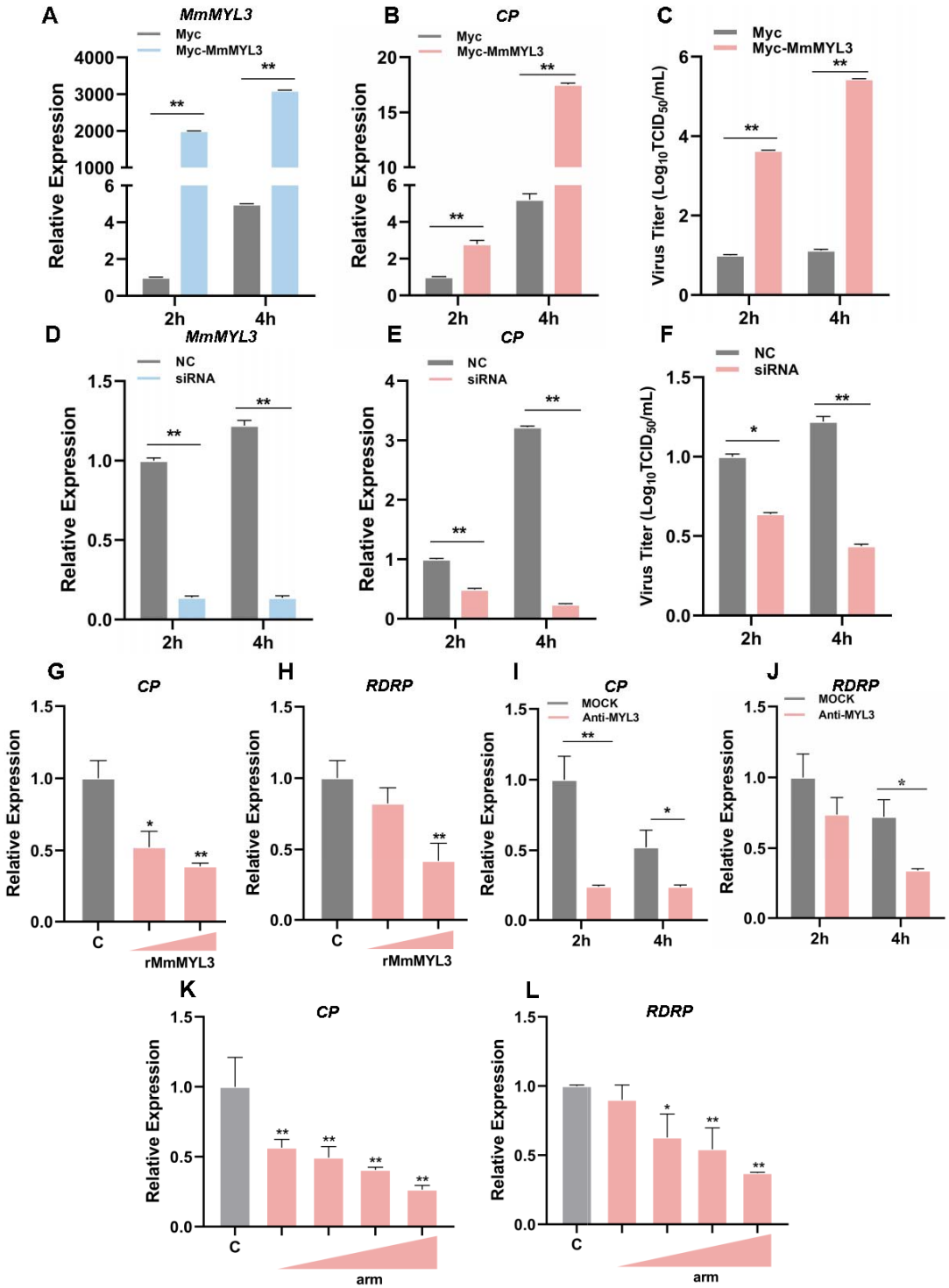

Fig.3. Effect of MmMYL3 on RGNNV entry. (A and B) hMMES1 cells were transfected with MmMYL3-Myc or Myc plasmid (Control) and infected with RGNNV (MOI = 1) for 2 and 4 h, respectively. Then, the cells were lysed for qRT-PCR to detect

the expression of MmMYL3 and CP. (C) Virus titer detection in MmMYL3-Myc transfected hMMES1 cells post RGNNV infection for 2 and 4 h. (D and E) qRT-PCR analysis of MmMYL3 and CP expression in siMmMYL3- or control-transfected hMMES1 cells infected with RGNNV for 2 and 4 h. (F) Virus titer detection in siMmMYL3 transfected hMMES1 cells post RGNNV infection for 2 and 4 h. (G and H) RGNNV was incubated with purified MmMYL3-GST proteins (100 or 500 ng) for 4 h at 4˚C, then was added to hMMES1 cells which were further incubated for 4 h at 4˚C. Cells were washed with PBS for three times and harvested for CP (G) and RDRP (H) expression detection. (I and J) hMMES1 cells were incubated with commercial anti-human MYL3 abs (1:50) for 4 h and then infected with RGNNV for 2 or 4 h at 4˚C. After washed with PBS for three times, cells were harvested for CP (I) and RDRP (J) expression detection. (K and L) hMMES1 cells were treated with different concentrations of arm peptides for 2 h at 4˚C, and after RGNNV infection for 4 h, CP (K) and RDRP (L) expression were detected by qRT-PCR. The results are presented as mean ± SD. Statistical significance was determined by an unpaired two-tailed Student's t test. *$P < 0.05$, **$P < 0.01$. Data are representative of three independent experiments.

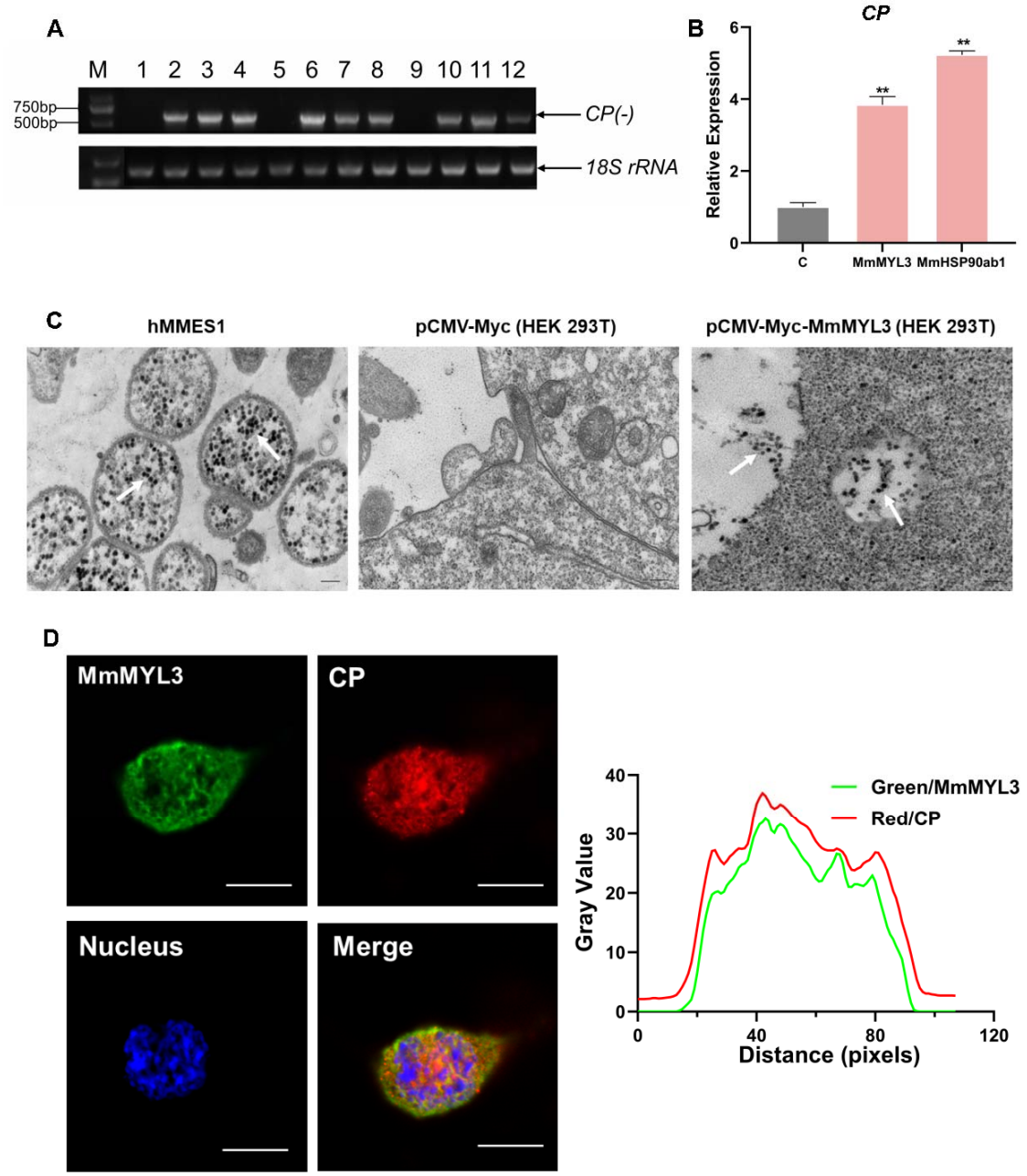

Fig.4. MmMYL3 was involved in RGNNV internalization. (A) RT-PCR analysis of CP (-) sequence. HEK293T cells were transfected with Myc empty vector (lines 1, 5, and 9), MmMYL3-Myc (lines 2, 6, and 10), MmHSP90ab1-Myc (lines 3, 7 and 11), or both

MmMYL3-Myc and MmHSP90ab1-Myc (lines 4, 8, and 12) plasmids for 24 h, respectively. Then cells were infected with RGNNV (MOI = 5) for 4 h. Next, the cells were washed to remove any unbound viruses and incubated for 24 h (lines 1–4), 48 h (lines 5–8) and 72 h (lines 9–12). Cells were harvested and total RNA was extracted for CP (-) detection by RT-PCR. Human 18S rRNA was detected as a reference. (B) HEK293T cells were transfected with MmMYL3-Myc, MmHSP90ab1-Myc or Myc plasmids, respectively. Then, transfected cells were infected with RGNNV (MOI = 5) for 24 h. Next, the cells were washed to remove any unbound viruses and total RNA was extracted for CP detection by qRT-PCR. (C) Transmission electron micrograph of RGNNV-infected hMMES1 cells and HEK293T cells transfected with Myc empty vector or MmMYL3-Myc with 80,000 magnifications. Bar = 200 nm. (D) HEK293T cells transfected with Myc empty vector or MmMYL3-Myc were infected with RGNNV (MOI = 5) for 24 h, CP (red) and MmMYL3 (green) were detected by immunofluorescence staining. Cell nuclei were stained with DAPI. Bar = 10 μm. Data were collected from three independent experiments and presented as mean ± SD. All results are representative of three similar experiments. **, $P < 0.01$.

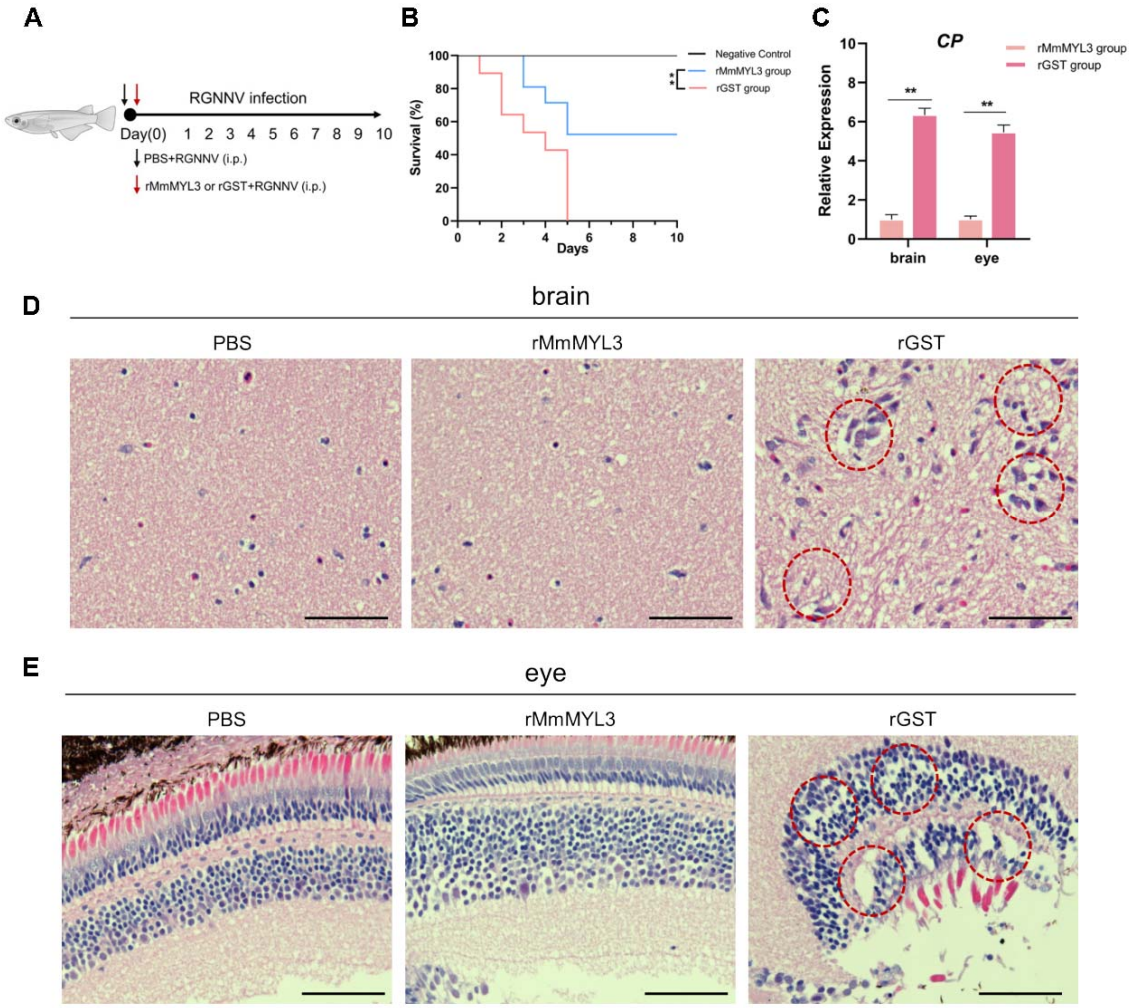

Fig.5. Recombinant MmMYL3 protein treatment protects marine medaka from RGNNV pathogenesis. (A) Schematic representation of the experimental design. RGNNV (100 $TCID_{50}$) was incubated with purified GST-tagged MmMYL3 recombinant protein (rMmMYL3, 500 ng) or GST protein (rGST, 500 ng) for 4 h at 4˚C. Marine medaka were infected with rMmMYL3-RGNNV or GST-RGNNV mixture by intraperitoneal (i.p.) injection, respectively. The negative control group of fishes were injected with the same volume of PBS. (B) Survival rates of marine medaka infected with RGNNV and MmMYL3 or GST protein mixtures. The cumulative survival rate was determined from 1 to 10 days post-infection. **, (P<0.01). (C) Quantification of RGNNV CP expression in brain and eye tissues by qRT-PCR. Data are represented as mean ± SD.

853 **, ($P < 0.01$). (D and E) Histopathological analysis of the eye (D) and brain (E) tissues
854 of fish treated with PBS, rMmMYL3, or rGST. Marine medaka were necropsied and the
855 eyes and brains were collected at day 5 post infection. Hematoxylin and eosin (H&E)
856 staining was used to assess tissue integrity. The vacuolization in eyes and brains were
857 marked by red dotted circle. Bar= 100 µm.

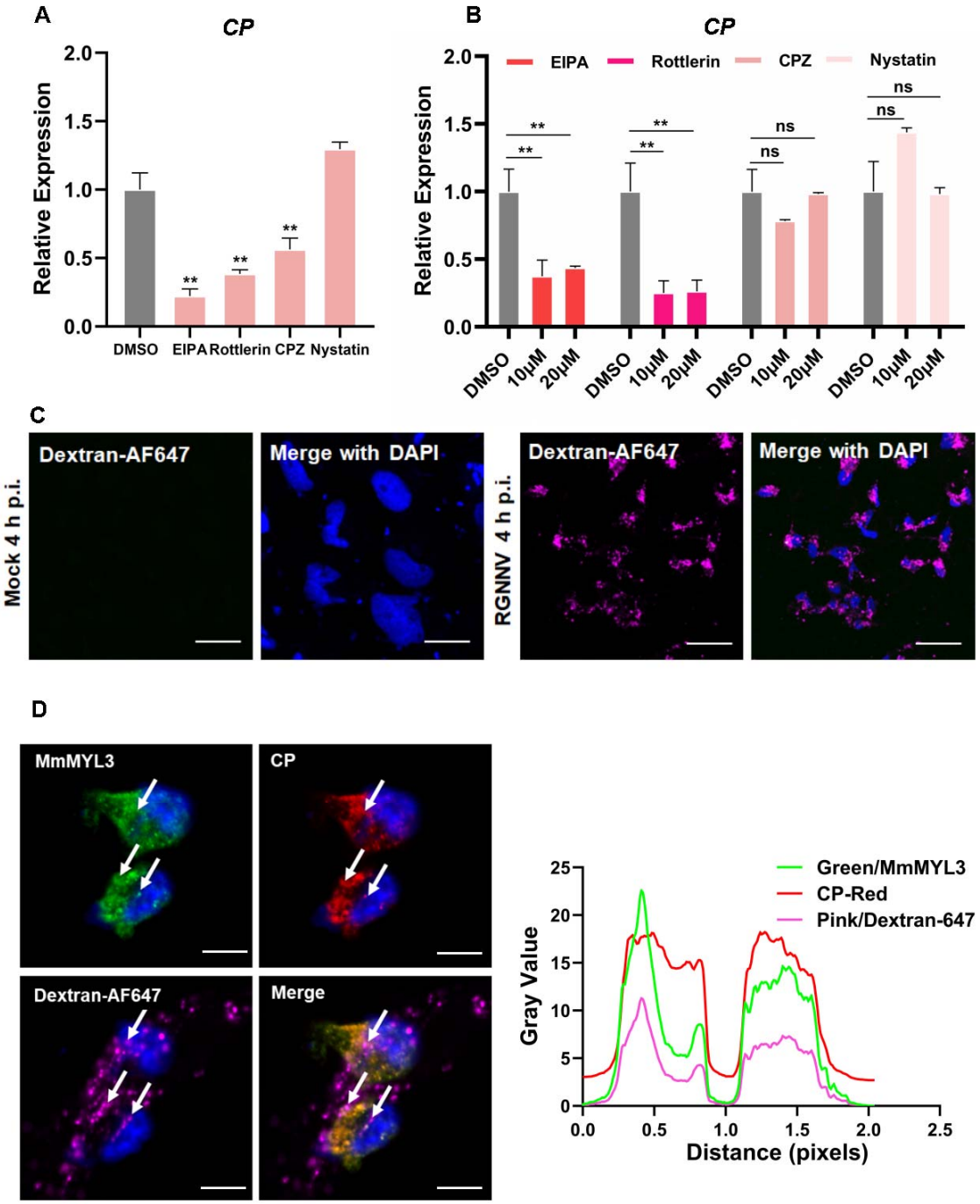

Fig.6. RGNNV triggers macropinocytosis mediated by MmMYL3. (A) Cells pretreated with EIPA, Rottlerin, CPZ or Nystatin were infected with RGNNV (MOI = 1) for 4 h at 28°C and the expression of CP was analyzed by qRT-PCR. (B) MmMYL3-

overexpressing hMMES1 cells were treated with different inhibitors and incubated with RGNNV (MOI = 1) for 4 h at 28°C, the expression of CP was analyzed by qRT-PCR. (C) hMMES1 cells were mock-infected or infected with RGNNV (MOI= 1) in medium containing Alexa Fluor 647-conjugated dextran (10,000 MW). At 4 hpi, cells were fixed and nuclei counterstained with DAPI, and imaged on a confocal microscope. Bar =10 μm. (D) Co-localization of MmMYL3 (green), RGNNV CP (red) and dextran-AF647 in RGNNV-infected hMMES1 cells. Cell nuclei were stained with DAPI. Bar =10 μm. Data were collected from three independent experiments and presented as mean ± SD. All results are representative of three similar experiments. ns, not significant; **, $P < 0.01$.

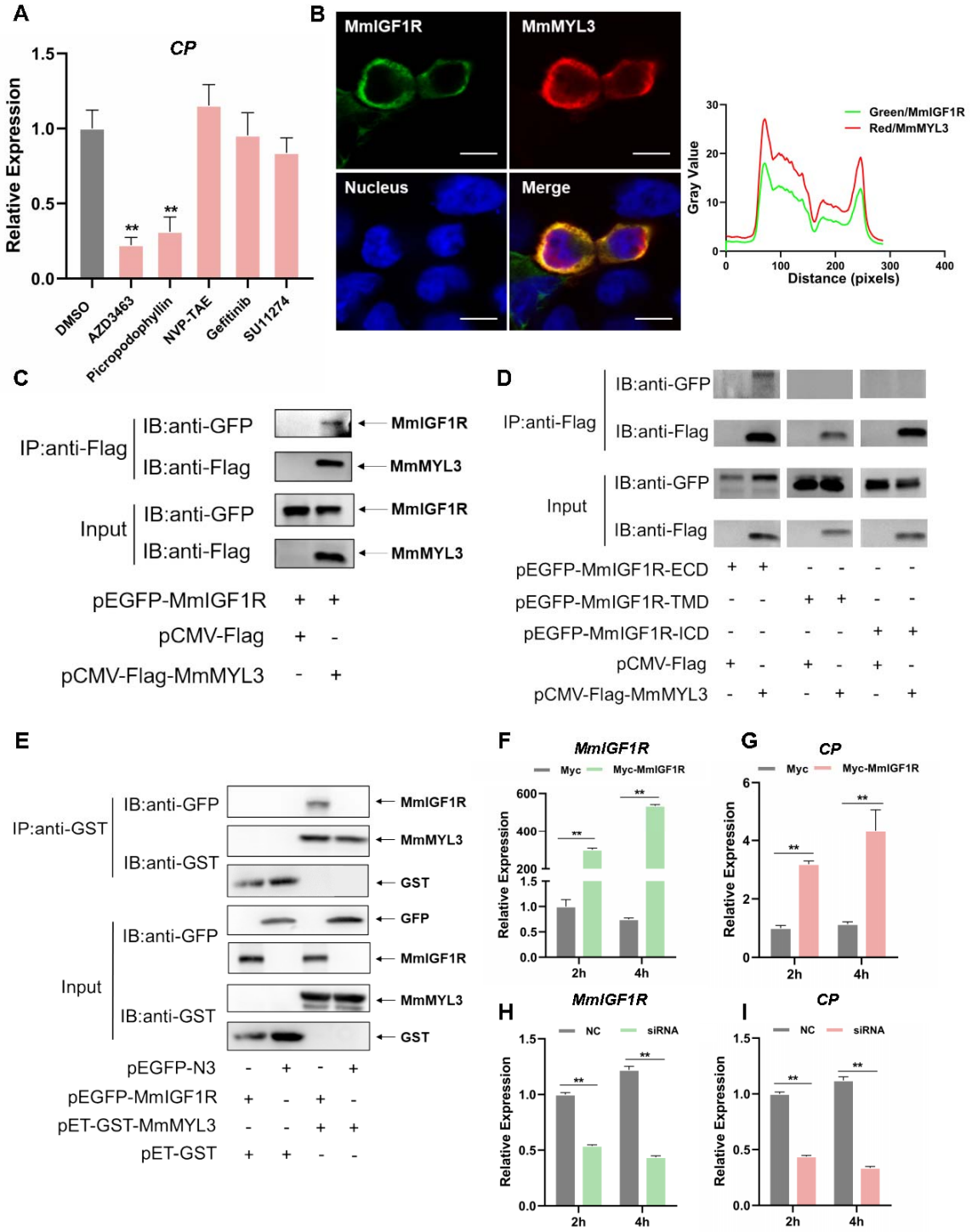

Fig.7. MmIGF1R is involved in MmMYL3 mediated RGNNV internalization. (A) MmMYL3-overexpressing hMMES1 cells were treated with different RTKs inhibitors, and incubated with RGNNV for 4 h at 28°C, the expression of CP was analyzed by qRT-

PCR. (B) MmIGF1R-GFP and MmMYL3-Myc were transfected into HEK293T cells as indicated for immunofluorescence analysis by using anti-Myc (red) abs. Nuclei were stained with DAPI. Bar =10 μm. (C and D) Immunoprecipitation (IP) (with anti-Flag) and immunoblot analysis (with anti-Flag and anti-GFP) of HEK293 cells transfected with plasmids encoding MmMYL3-Flag, MmIGF1R-GFP, MmIGF1R-ECD-GFP, MmIGF1R-TMD-GFP or MmIGF1R-ICD-GFP for 48 h. (E) The lysates of HEK293T cells transfected with indicated plasmids were pulled down with purified MmMYL3-GST or GST proteins. The proteins bound to MmIGF1R and the input were immunoblotted with anti-GST and anti-GFP abs. (F and G) hMMES1 cells were transfected with MmIGF1R-GFP or GFP-N3 plasmid (Control) and infected with RGNNV (MOI = 1) for 2 and 4 h respectively. Then, the cells were lysed for qRT-PCR to detect the expression of MmIGF1R and CP. (H and I) qRT-PCR analysis of MmIGF1R and CP mRNA expression of siMmIGF1R- or NC (control)-transfected hMMES1 cells, following infection with RGNNV for 2 and 4 h.Data were collected from three independent experiments and presented as mean ± SD. All results are representative of three similar experiments. **, $P < 0.01$.

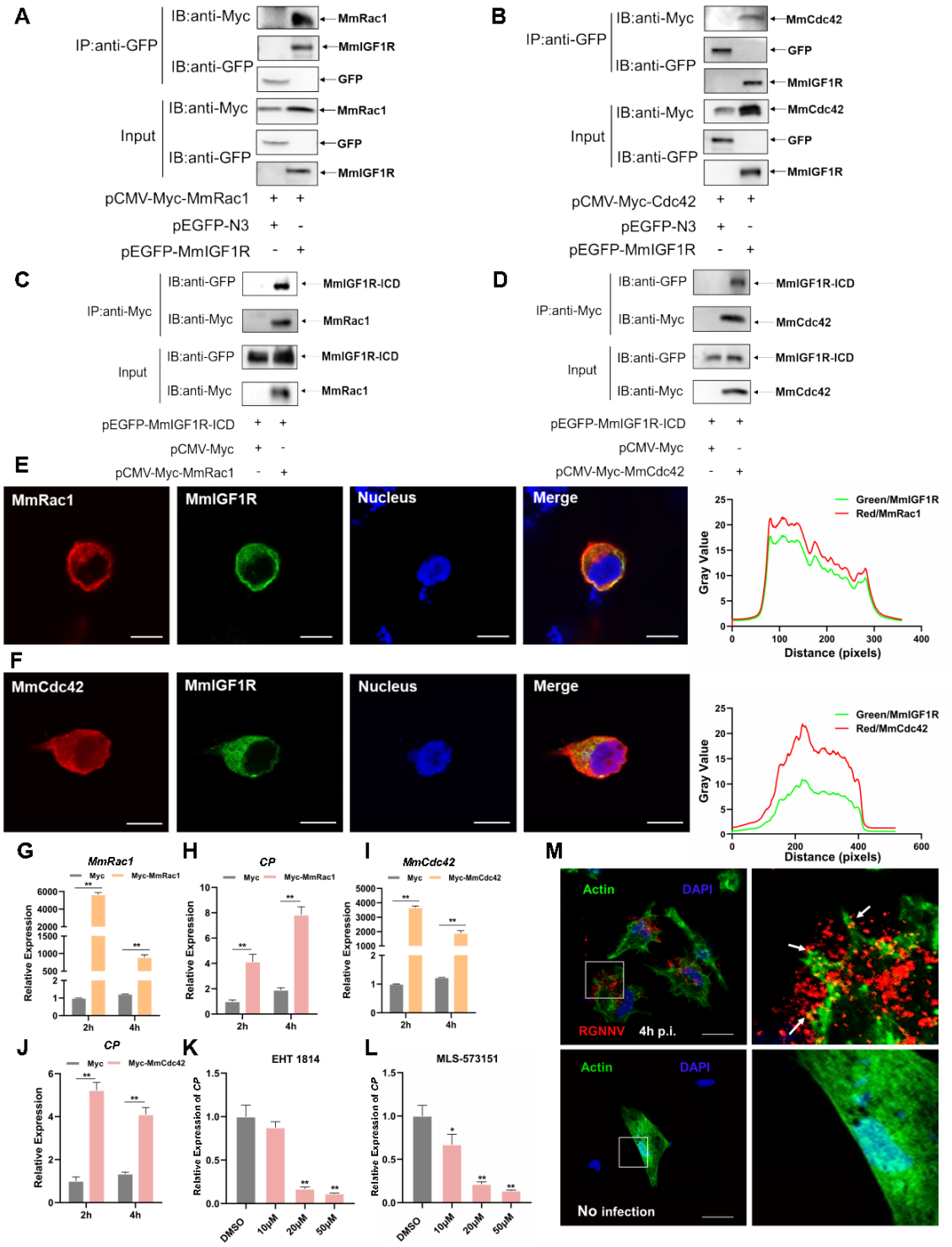

Fig.8. MmRac1 and MmCdc42 regulate RGNNV entry. (A and B) HEK293T cells were transfected with MmIGF1R-GFP and MmRac1-Myc or MmCdc42-Myc plasmids as indicated for 48 h, and the cell lysates were subjected to coimmunoprecipitation analysis

with anti-GFP magnetic beads as described above. (C and D) HEK293T cells were transfected with MmRac1-Myc, MmCdc42-Myc and MmIGF1R-ICD-GFP plasmids, respectively. At 48 h posttransfection, the cell lysates were subjected to coimmunoprecipitation analysis with anti-Myc magnetic beads as indicated. (E and F) MmIGF1R-GFP and MmRac1-Myc or MmCdc42-Myc were transfected into HEK293T cells as indicated for immunofluorescence analysis by using anti-Myc (red) antibodies. Nuclei were stained with DAPI. Bar = 10 μm. (G-J) hMMES1 cells were transfected with MmRac1-Myc, MmCdc42-Myc or pCMV-Myc (Control) plasmids and infected with RGNNV (MOI = 1) for 2 and 4 h respectively. Then, the cells were lysed for qRT-PCR to detect the expression of MmRac1, MmCdc42 and CP. (K and L) hMMES1 cells were treated with inhibitors of Rac1 (EHT1814) or Cdc42 (MLS-573151) for 4 h, then infected with RGNNV (MOI=1) for 4 h at 28°C, the cells were lysed for qRT-PCR to detect the expression of CP. (M) Actin cytoskeleton dynamics are involved in RGNNV entry. hMMES1 cells were exposed to RGNNV (MOI = 1) or PBS for 4 h and actin filaments were labeled with iFluorTM 488 phalloidin (green), then fixed, and permeabilized as described above. Nuclei were stained with DAPI. Images were captured with a 100× oil immersion objective. A higher magnification of the boxed area reveals the formation of actin protrusions at the cell surface membrane (arrows). Bar =10 μm. Data were collected from three independent experiments and presented as mean ± SD. All results are representative of three similar experiments. *, $P < 0.05$; **, $P < 0.01$.

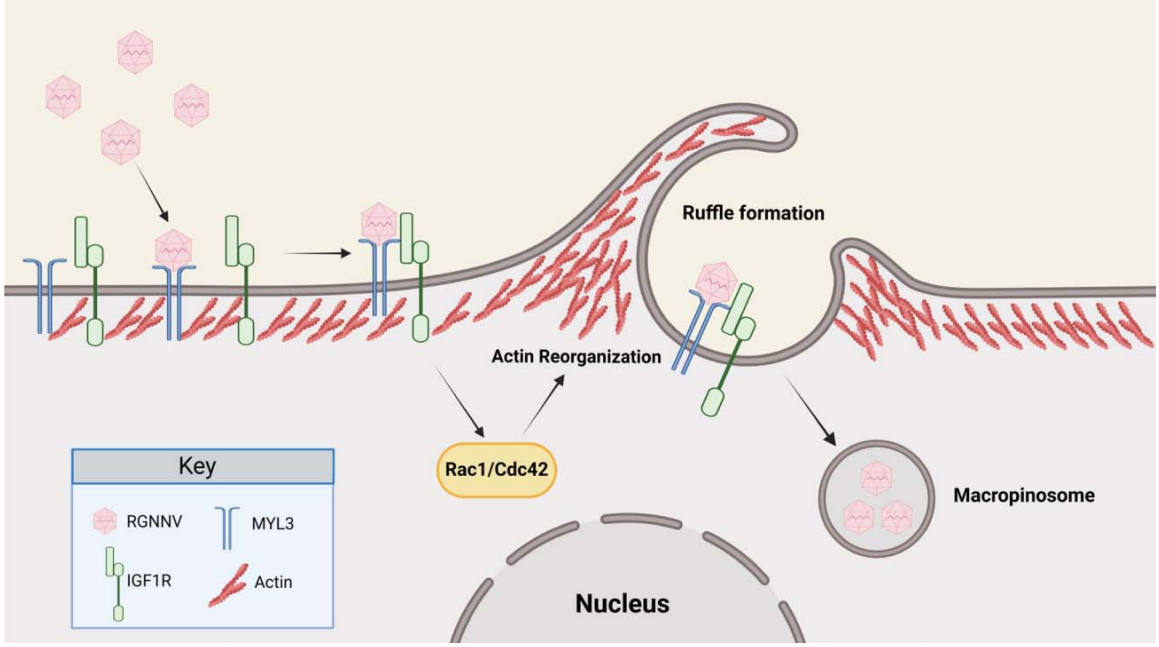

Fig. 9. Model of RGNNV entry into host cells via macropinocytosis mediated by MmMYL3. RGNNV particles engage hMMES1 cells through interactions between CP and MYL3, a receptor on the cell surface, which is followed by interactions between MYL3 and IGF1R. Then, IGF1R activates and recruits small GTPases Rac1/Cdc42 to induce actin reorganization, facilitate the internalization of RGNNV via macropinocytosis.

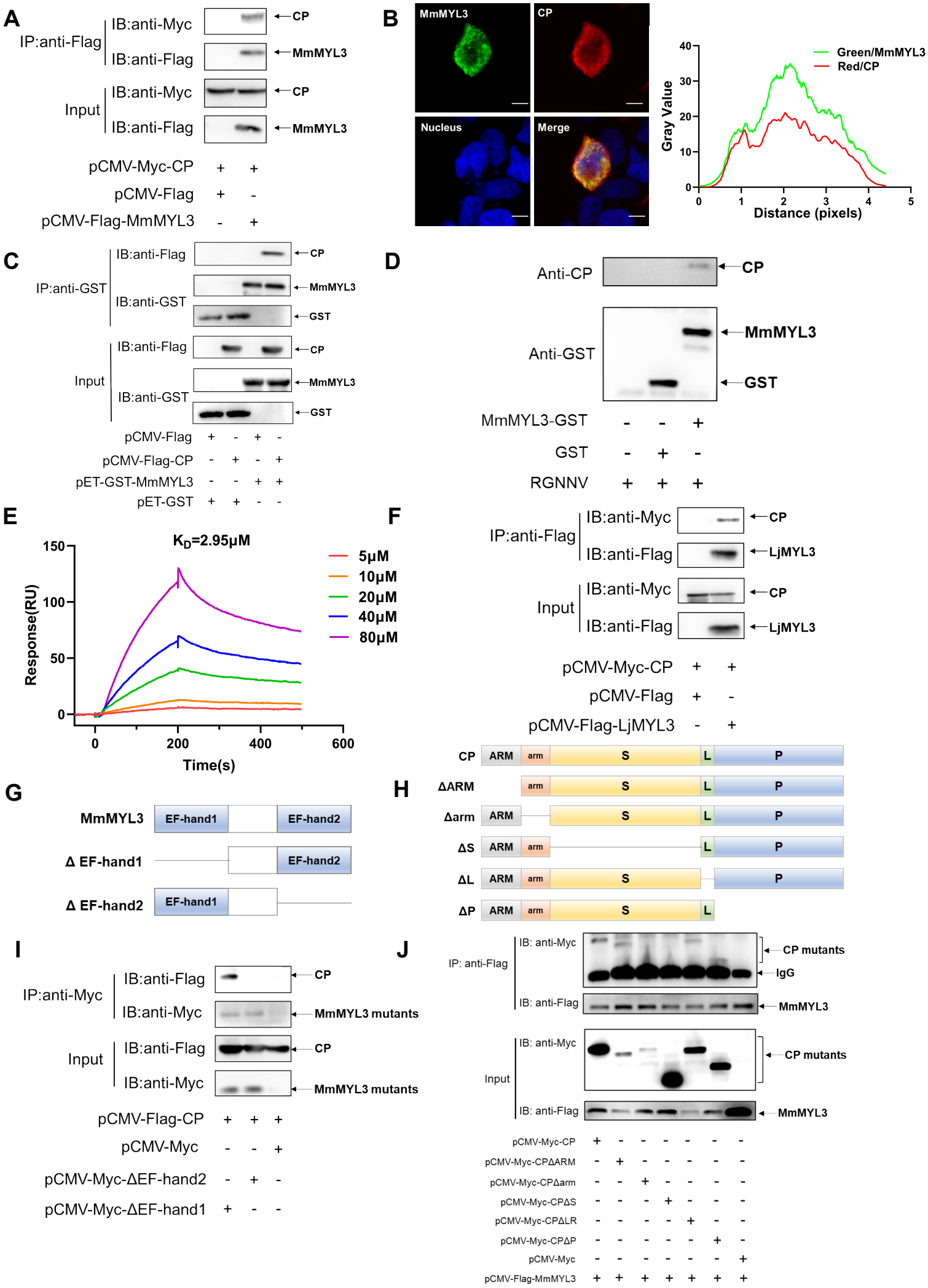
A
IP:anti-Flag
IB:anti-Myc
IB:anti-Flag
Input
IB:anti-Myc
IB:anti-Flag
CP
MmMYL3
CP
MmMYL3
pCMV-Myc-CP + +
pCMV-Flag + -
pCMV-Flag-MmMYL3 - +
B
MmMYL3
CP
Nucleus
Merge
Green/MmMYL3
Red/CP
Gray Value
Distance (pixels)
C
IP:anti-GST
IB:anti-Flag
IB:anti-GST
Input
IB:anti-Flag
IB:anti-GST
CP
MmMYL3
GST
CP
MmMYL3
GST
pCMV-Flag + - + -
pCMV-Flag-CP - + - +
pET-GST-MmMYL3 - - + +
pET-GST + + - -
D
Anti-CP
Anti-GST
CP
MmMYL3
GST
MmMYL3-GST - - +
GST - + -
RGNNV + + +
E
K_D=2.95μM
Response(RU)
Time(s)
5μM
10μM
20μM
40μM
80μM
F
IP:anti-Flag
IB:anti-Myc
IB:anti-Flag
Input
IB:anti-Myc
IB:anti-Flag
CP
LjMYL3
CP
LjMYL3
pCMV-Myc-CP + +
pCMV-Flag + -
pCMV-Flag-LjMYL3 - +
G
MmMYL3
EF-hand1
EF-hand2
Δ EF-hand1
EF-hand2
Δ EF-hand2
EF-hand1
H
CP
ΔARM
Δarm
ΔS
ΔL
ΔP
ARM
arm
S
L
P
I
IP:anti-Myc
IB:anti-Flag
IB:anti-Myc
Input
IB:anti-Flag
IB:anti-Myc
CP
MmMYL3 mutants
CP
MmMYL3 mutants
pCMV-Flag-CP + + +
pCMV-Myc - - +
pCMV-Myc-ΔEF-hand2 - + -
pCMV-Myc-ΔEF-hand1 + - -
J
IP: anti-Flag
IB: anti-Myc
IB: anti-Flag
Input
IB: anti-Myc
IB: anti-Flag
CP mutants
IgG
MmMYL3
CP mutants
MmMYL3
pCMV-Myc-CP + - - - - - -
pCMV-Myc-CPΔARM - + - - - - -
pCMV-Myc-CPΔarm - - + - - - -
pCMV-Myc-CPΔS - - - + - - -
pCMV-Myc-CPΔLR - - - - + - -
pCMV-Myc-CPΔP - - - - - + -
pCMV-Myc - - - - - - +
pCMV-Flag-MmMYL3 + + + + + + +

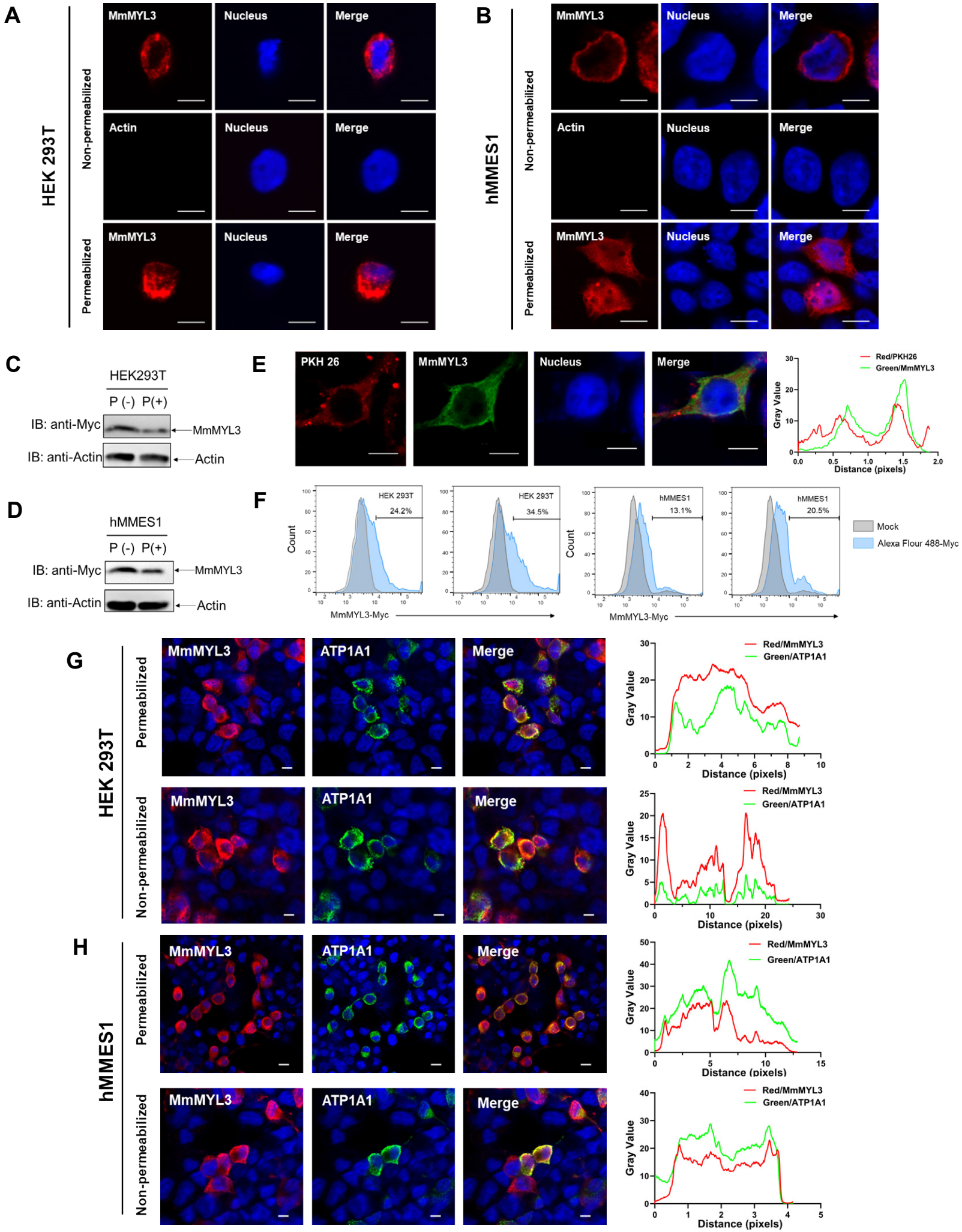
A
HEK 293T
Non-permeabilized
Permeabilized
MmMYL3
Nucleus
Merge
Actin
B
hMMES1
C
HEK293T
P (-) P(+)
IB: anti-Myc
IB: anti-Actin
MmMYL3
Actin
D
hMMES1
E
PKH 26
Red/PKH26
Green/MmMYL3
Gray Value
Distance (pixels)
F
HEK 293T
24.2%
34.5%
hMMES1
13.1%
20.5%
Count
MmMYL3-Myc
Mock
Alexa Flour 488-Myc
G
ATP1A1
Red/MmMYL3
Green/ATP1A1
H

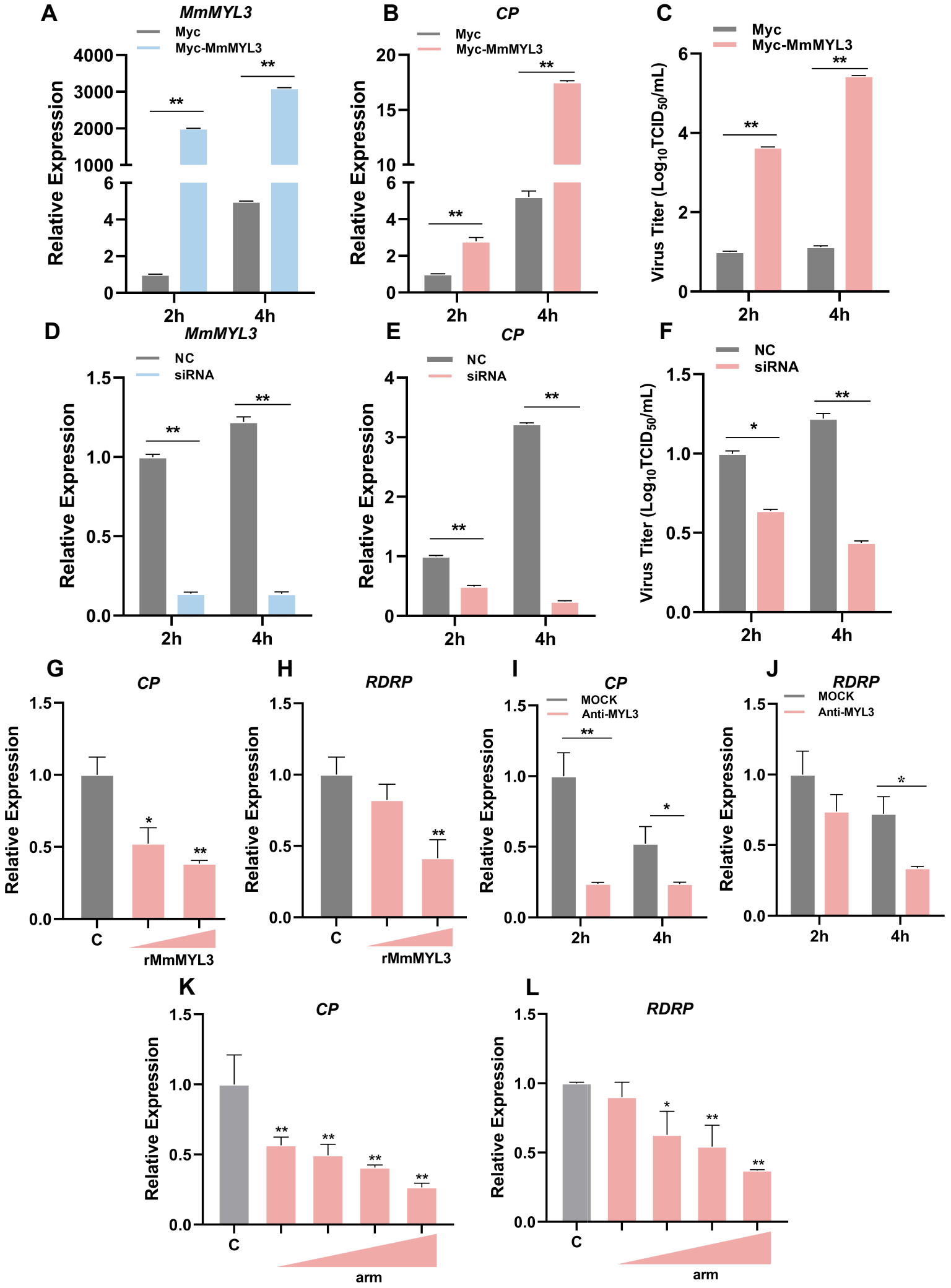
A
MmMYL3
Myc
Myc-MmMYL3
Relative Expression
4000
3000
2000
1000
6
4
2
0
**
**
2h
4h
B
CP
Myc
Myc-MmMYL3
Relative Expression
20
15
10
6
4
2
0
**
**
2h
4h
C
Myc
Myc-MmMYL3
Virus Titer (Log10TCID50/mL)
6
4
2
0
**
**
2h
4h
D
MmMYL3
NC
siRNA
Relative Expression
1.5
1.0
0.5
0.0
**
**
2h
4h
E
CP
NC
siRNA
Relative Expression
4
3
2
1
0
**
**
2h
4h
F
NC
siRNA
Virus Titer (Log10TCID50/mL)
1.5
1.0
0.5
0.0
*
**
2h
4h
G
CP
Relative Expression
1.5
1.0
0.5
0.0
*
**
C
rMmMYL3
H
RDRP
Relative Expression
1.5
1.0
0.5
0.0
**
C
rMmMYL3
I
CP
MOCK
Anti-MYL3
Relative Expression
1.5
1.0
0.5
0.0
**
*
2h
4h
J
RDRP
MOCK
Anti-MYL3
Relative Expression
1.5
1.0
0.5
0.0
*
2h
4h
K
CP
Relative Expression
1.5
1.0
0.5
0.0
**
**
**
**
C
arm
L
RDRP
Relative Expression
1.5
1.0
0.5
0.0
*
**
**
C
arm

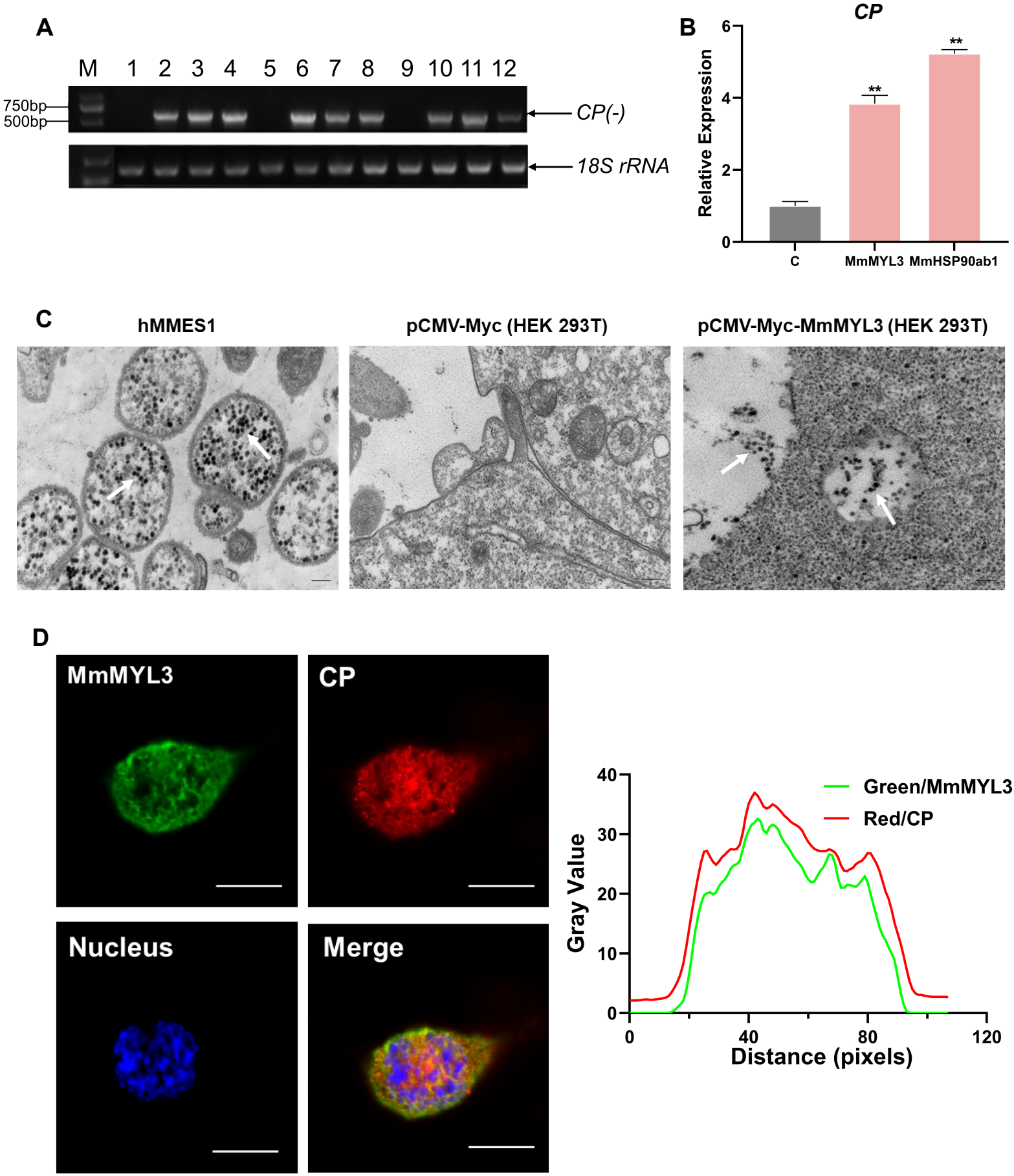
A
M 1 2 3 4 5 6 7 8 9 10 11 12
750bp
500bp
CP(-)
18S rRNA
B
CP
Relative Expression
0
2
4
6
**
**
C
MmMYL3
MmHSP90ab1
C
hMMES1
pCMV-Myc (HEK 293T)
pCMV-Myc-MmMYL3 (HEK 293T)
D
MmMYL3
CP
Nucleus
Merge
Green/MmMYL3
Red/CP
Gray Value
0
10
20
30
40
0
40
80
120
Distance (pixels)

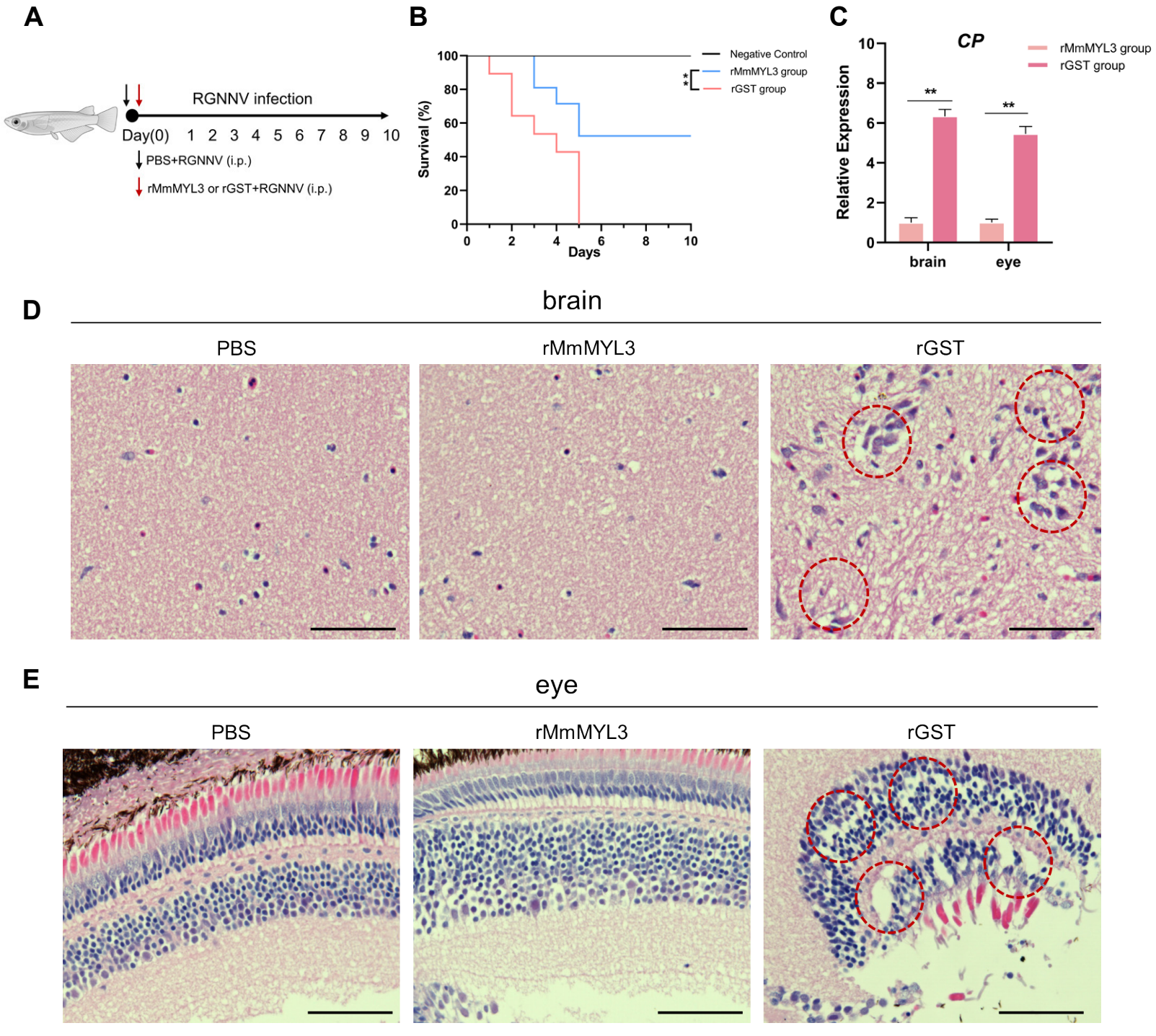
A
RGNNV infection
Day(0) 1 2 3 4 5 6 7 8 9 10
PBS+RGNNV (i.p.)
rMmMYL3 or rGST+RGNNV (i.p.)
B
Survival (%)
Days
Negative Control
rMmMYL3 group
rGST group
**
C
CP
Relative Expression
rMmMYL3 group
rGST group
**
**
brain
eye
D
brain
PBS
rMmMYL3
rGST
E
eye
PBS
rMmMYL3
rGST

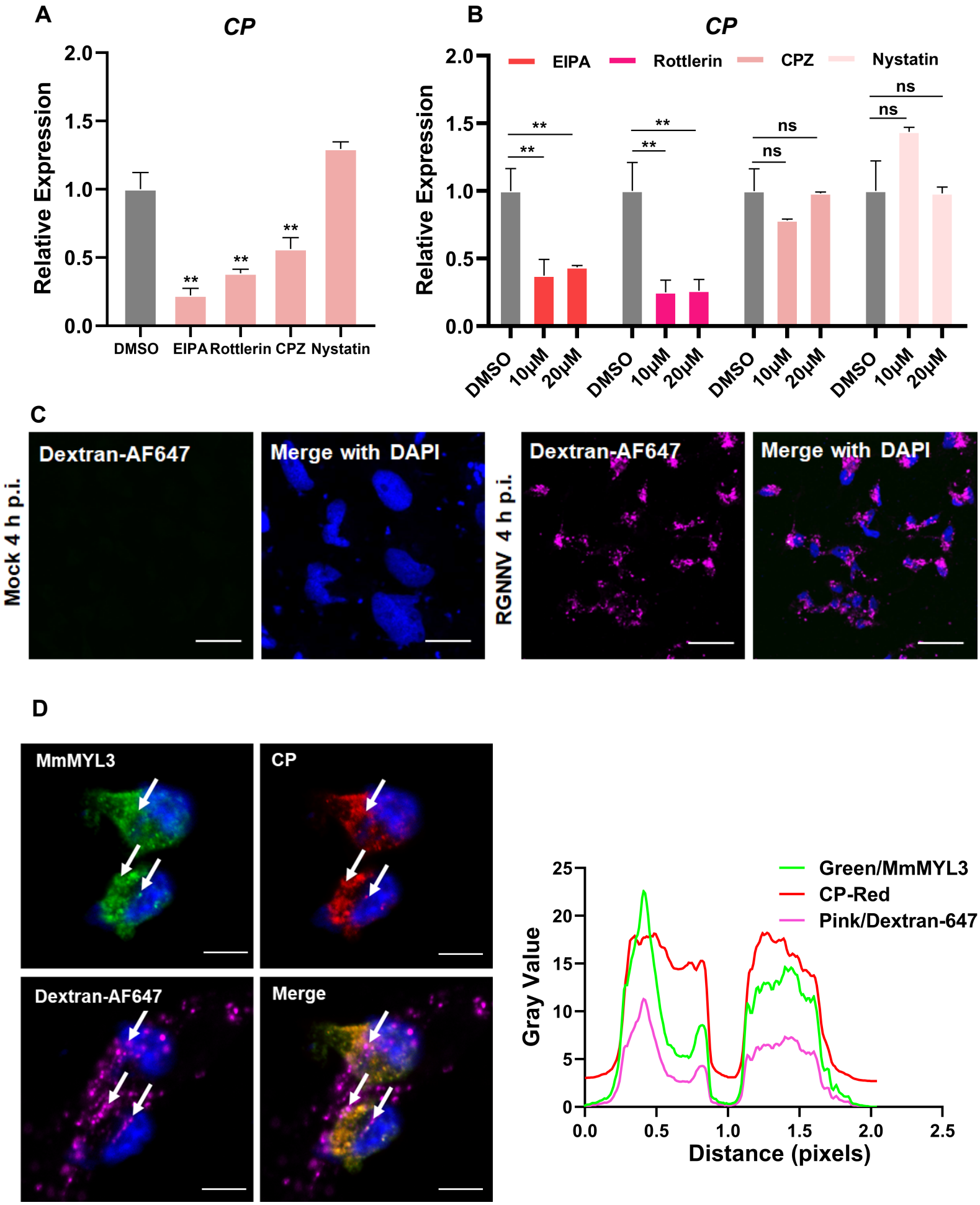
A
CP
Relative Expression
2.0
1.5
1.0
0.5
0.0
**
**
**
DMSO
EIPA
Rottlerin
CPZ
Nystatin
B
CP
EIPA
Rottlerin
CPZ
Nystatin
ns
**
DMSO
10μM
20μM
C
Mock 4 h p.i.
RGNNV 4 h p.i.
Dextran-AF647
Merge with DAPI
D
MmMYL3
CP
Dextran-AF647
Merge
Green/MmMYL3
CP-Red
Pink/Dextran-647
Gray Value
Distance (pixels)
25
20
15
10
5
0
0.0
0.5
1.0
1.5
2.0
2.5

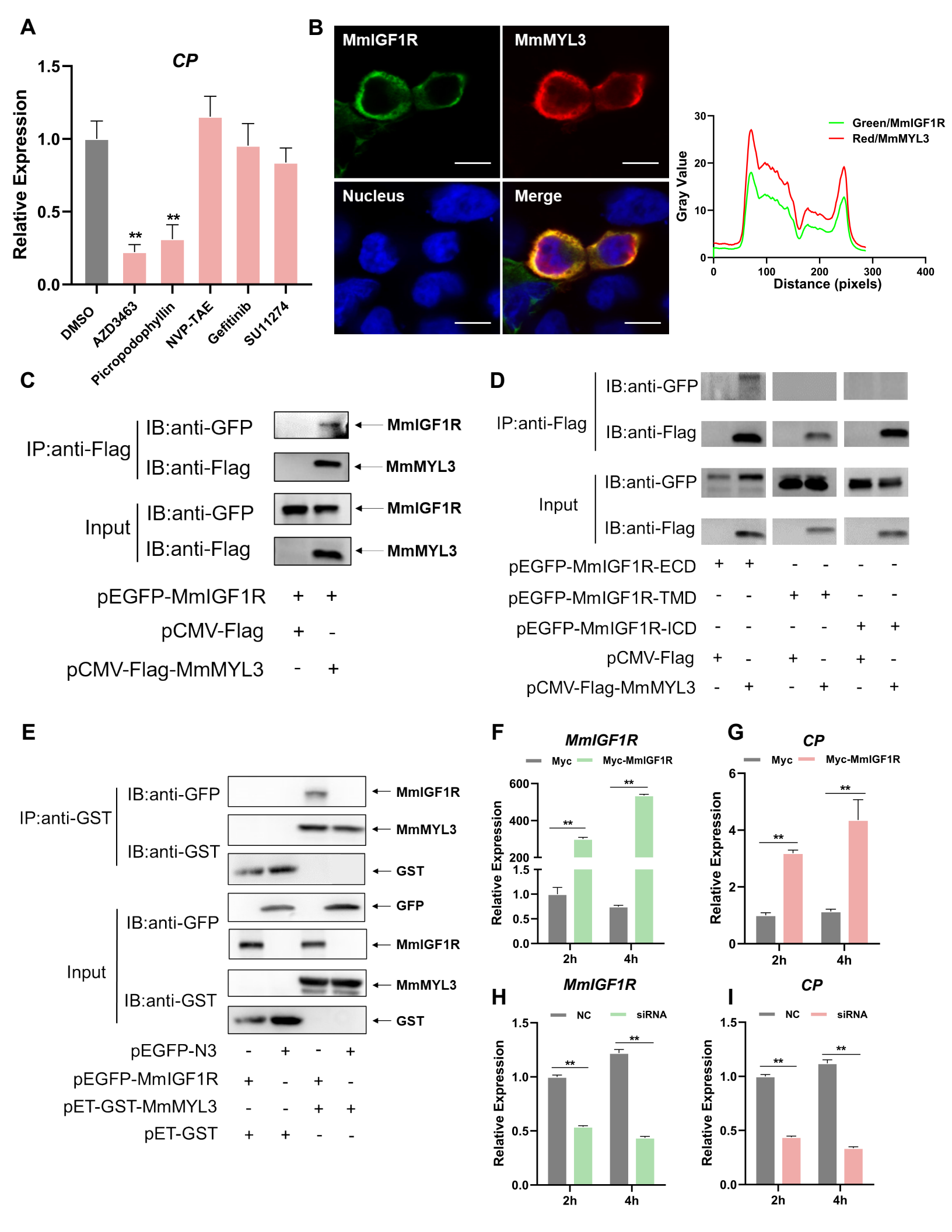
A
CP
Relative Expression
1.5
1.0
0.5
0.0
**
**
DMSO
AZD3463
Picropodophyllin
NVP-TAE
Gefitinib
SU11274
B
MmIGF1R
MmMYL3
Nucleus
Merge
Green/MmIGF1R
Red/MmMYL3
Gray Value
Distance (pixels)
C
IP:anti-Flag
IB:anti-GFP
IB:anti-Flag
Input
IB:anti-GFP
IB:anti-Flag
MmIGF1R
MmMYL3
MmIGF1R
MmMYL3
pEGFP-MmIGF1R + +
pCMV-Flag + -
pCMV-Flag-MmMYL3 - +
D
IP:anti-Flag
IB:anti-GFP
IB:anti-Flag
Input
IB:anti-GFP
IB:anti-Flag
pEGFP-MmIGF1R-ECD + + - - - -
pEGFP-MmIGF1R-TMD - - + + - -
pEGFP-MmIGF1R-ICD - - - - + +
pCMV-Flag + - + - + -
pCMV-Flag-MmMYL3 - + - + - +
E
IP:anti-GST
IB:anti-GFP
IB:anti-GST
Input
IB:anti-GFP
IB:anti-GST
MmIGF1R
MmMYL3
GST
GFP
MmIGF1R
MmMYL3
GST
pEGFP-N3 - + - +
pEGFP-MmIGF1R + - + -
pET-GST-MmMYL3 - - + +
pET-GST + + - -
F
MmIGF1R
Myc
Myc-MmIGF1R
Relative Expression
600
400
200
1.5
1.0
0.5
0.0
**
**
2h
4h
G
CP
Myc
Myc-MmIGF1R
Relative Expression
6
4
2
0
**
**
2h
4h
H
MmIGF1R
NC
siRNA
Relative Expression
1.5
1.0
0.5
0.0
**
**
2h
4h
I
CP
NC
siRNA
Relative Expression
1.5
1.0
0.5
0.0
**
**
2h
4h

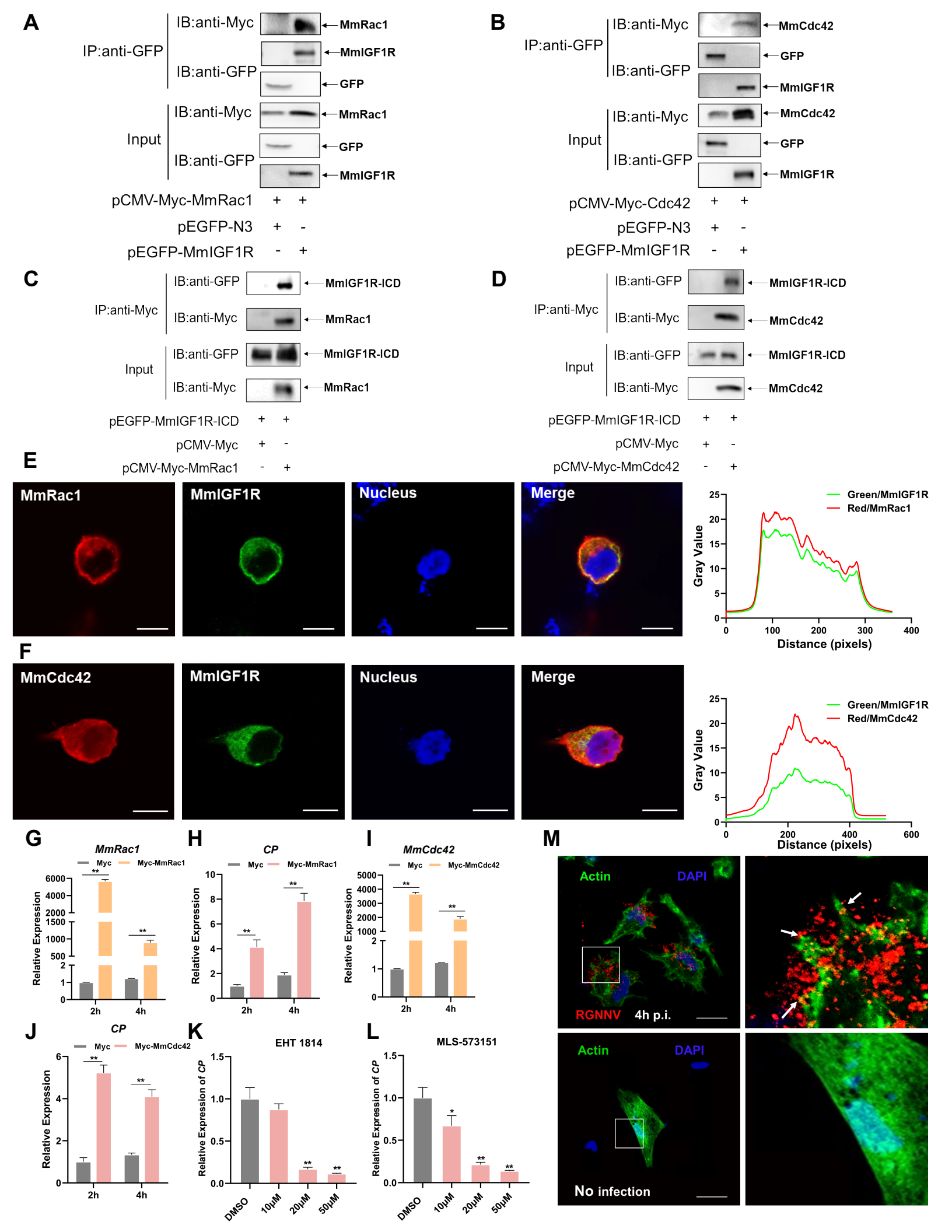
A
IP:anti-GFP
IB:anti-Myc
MmRac1
IB:anti-GFP
MmIGF1R
GFP
Input
IB:anti-Myc
MmRac1
IB:anti-GFP
GFP
MmIGF1R
pCMV-Myc-MmRac1 + +
pEGFP-N3 + -
pEGFP-MmIGF1R - +
B
IP:anti-GFP
IB:anti-Myc
MmCdc42
IB:anti-GFP
GFP
MmIGF1R
Input
IB:anti-Myc
MmCdc42
IB:anti-GFP
GFP
MmIGF1R
pCMV-Myc-Cdc42 + +
pEGFP-N3 + -
pEGFP-MmIGF1R - +
C
IP:anti-Myc
IB:anti-GFP
MmIGF1R-ICD
IB:anti-Myc
MmRac1
Input
IB:anti-GFP
MmIGF1R-ICD
IB:anti-Myc
MmRac1
pEGFP-MmIGF1R-ICD + +
pCMV-Myc + -
pCMV-Myc-MmRac1 - +
D
IP:anti-Myc
IB:anti-GFP
MmIGF1R-ICD
IB:anti-Myc
MmCdc42
Input
IB:anti-GFP
MmIGF1R-ICD
IB:anti-Myc
MmCdc42
pEGFP-MmIGF1R-ICD + +
pCMV-Myc + -
pCMV-Myc-MmCdc42 - +
E
MmRac1
MmIGF1R
Nucleus
Merge
Green/MmIGF1R
Red/MmRac1
Gray Value
Distance (pixels)
F
MmCdc42
MmIGF1R
Nucleus
Merge
Green/MmIGF1R
Red/MmCdc42
Gray Value
Distance (pixels)
G
MmRac1
Myc
Myc-MmRac1
Relative Expression
2h
4h
H
CP
Myc
Myc-MmRac1
Relative Expression
2h
4h
I
MmCdc42
Myc
Myc-MmCdc42
Relative Expression
2h
4h
J
CP
Myc
Myc-MmCdc42
Relative Expression
2h
4h
K
EHT 1814
Relative Expression of CP
DMSO
10μM
20μM
50μM
L
MLS-573151
Relative Expression of CP
DMSO
10μM
20μM
50μM
M
Actin
DAPI
RGNNV
4h p.i.
Actin
DAPI
No infection

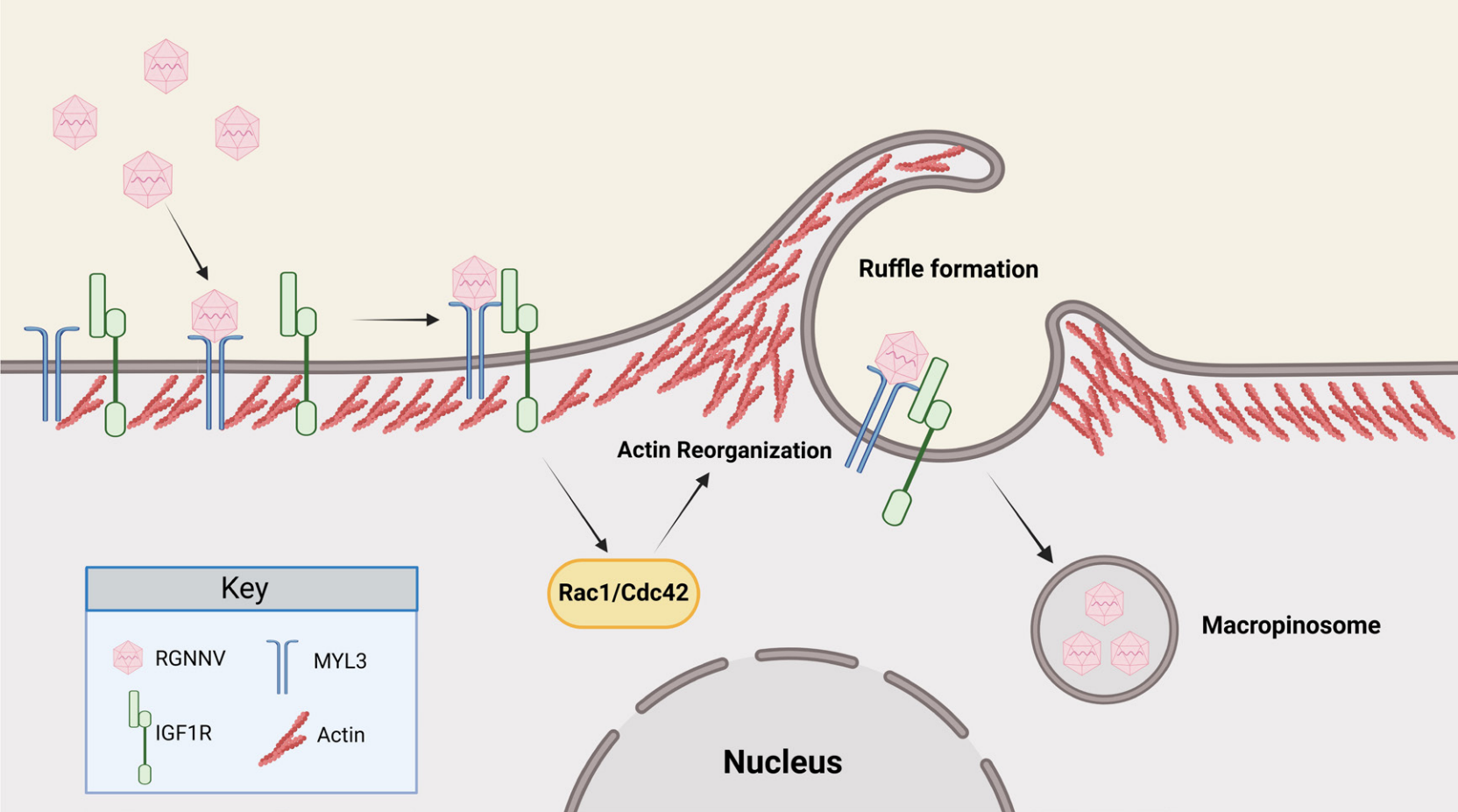
Ruffle formation
Actin Reorganization
Rac1/Cdc42
Macropinosome
Nucleus
Key
RGNNV
MYL3
IGF1R
Actin